Article:

Vafaei, S and Wen, D (2015) Modification of the Young-Laplace equation and prediction of bubble interface in the presence of nanoparticles. Advances in Colloid and Interface Science, 225. pp. 1-15. ISSN 0001-8686

https://doi.org/10.1016/j.cis.2015.07.006

Modification of the Young-Laplace equation and prediction of bubble interface in the presence of nanoparticles

Saeid Vafaei[1*], Dongsheng Wen [2]

[1]Department of Mechanical, Materials and Manufacturing, University of Nottingham, Nottingham, UK.

s.vafaei@qmul.ac.uk

[2]School of Process Environmental and Materials Science, University of Leeds, Leeds, UK.

d.wen@leeds.ac.uk

Abstract: Bubbles are fundamental to our daily life and have wide applications such as in the chemical and petrochemical industry, pharmaceutical engineering, mineral processing and colloids engineering. This paper reviews the existing theoretical and experimental bubble studies, with a special focus on the dynamics of triple line and the influence of nanoparticles on the bubble growth and departure process. Nanoparticles are found to influence significantly the effective interfacial properties and the dynamics of triple line, whose effects are dependent on the particle morphology and their interaction with the substrate. While the Young-Laplace equation is widely applied to predict the bubble shape, its application is limited under highly non-equilibrium conditions. Using gold nanoparticle as an example, new experimental study is conducted to reveal the particle concentration influence on the behaviour of triple line and bubble dynamics. A new method is developed to predict the bubble shape when the interfacial equilibrium conditions cannot be met, such as during the oscillation period. The method is used to calculate the pressure difference between the gas and liquid phase, which is shown to oscillate across the liquid-gas interface and is responsible for the interface fluctuation. The comparison of the theoretical study with the experimental data shows a very good agreement, which suggests its potential application to predict bubble shape during non-equilibrium conditions.

Keywords: Dynamics of bubble growth, Dynamics of triple line, Contact angle, Liquid-gas surface tension, Solid surface tensions, Gold nanoparticles, Nanofluids, Young-Laplace equation, Wettability, Bubble fluctuation, Oscillation.

Contents

1. Introduction

Nanofluids, functional nanoparticle dispersions, have been recently employed to enhance thermal management of miniaturized devices, ink jet printing, automobile industries, chemical and power plants, pharmaceutical industries and biomedical engineering. In many studies, nanoparticles have been observed to be able to modify thermal conductivity [1-2], viscosity [2-3], liquid-gas [4-6] and solid surface tensions [7] of the base fluid. The modification of the effective thermophysical properties influences the pressure drop and heat transfer coefficient in macro/microchannels [2]. The modification of liquid-gas and solid surface tensions would change the force balance at the triple line and consequently affect its dynamic behavior [7-8] including the radius of triple line [9] and the bubble contact angle [5, 10], which has significant effects on the bubble growth and departure process [11-16], as well as the boiling heat transfer [6, 17-24].

This paper reviews the existing experimental, analytical and numerical approaches, associated with the behavior of triple line and the dynamics of bubble growth and departure process, with and without the presence of nanoparticles. In addition, the Young-Laplace equation is modified to increase the accuracy of the bubble shape prediction when the equilibrium between gas and liquid is relatively weak, i.e., during the bubble fluctuation period when the shear stress is relatively high or in the departure period where the bubble is stretched upwards. A new method is developed to calculate the pressure difference between gas and liquid phases which is observed to oscillate across the liquid-gas interface, along the perimeter of bubble. In addition, the effects of gold nanoparticles on the liquid-gas surface tension, the dynamics of triple line, and the bubble growth and departure process are investigated experimentally.

2. Overview of the behaviour of triple line

The liquid-gas, σ_{lg}, solid-liquid, σ_{sl}, and solid-gas, σ_{sg} surface tensions are the major effective forces at the triple line, as shown schematically in Figure 1 (a, c) for bubbles and droplets respectively. The Young equation, $\sigma_{\mathrm{lg}} \cos\theta_{\mathrm{e}} = \sigma_{\mathrm{sg}} - \sigma_{\mathrm{sl}}$, demonstrates the force balance at the triple line traditionally, where θ_{e} is the equilibrium contact angle. The Young equation is associated with several restrictions and has never been experimentally verified for axisymmetric droplets. Its application is limited to the situations where the substrate is ideal [25-26] and the contact angle is size independent [27-28]. The Young equation cannot be applied directly except for long droplets [27]. The left side of the Young equation is size dependent, while the right side of the equation contains physical properties which make the equation inconsistent. The force balance between liquid-gas and solid surface tensions has a significant role on the behavior of triple line and consequently the interfacial shapes of bubbles and droplets.

The liquid-gas surface tension can be found for most of materials however the solid-liquid and solid-gas surface tensions are not easily available. Several independent approaches have been employed to calculate the solid surface tensions [26, 29], such as Berthelot's combining rule [30], $\sigma_{\mathrm{sl}} = (\sqrt{\sigma_{\mathrm{lg}}} - \sqrt{\sigma_{\mathrm{sg}}})^2$, the modified Berthelot's rule [31], $\sigma_{\mathrm{sl}} = \sigma_{\mathrm{lg}} + \sigma_{\mathrm{sg}} - 2\sqrt{\sigma_{\mathrm{lg}}\sigma_{\mathrm{sg}}}\exp - \beta(\sigma_{\mathrm{lg}} - \sigma_{\mathrm{sg}})^2$, the alternative formulation [32-33], $\sigma_{\mathrm{sl}} = \sigma_{\mathrm{lg}} + \sigma_{\mathrm{sg}} - 2\sqrt{\sigma_{\mathrm{sg}}\sigma_{\mathrm{lg}}}(1 - \beta_{\mathrm{o}}(\sigma_{\mathrm{lg}} - \sigma_{\mathrm{sg}})^2)$, and the equation of state formulation [34-35], $\sigma_{\mathrm{sl}} = \dfrac{(\sqrt{\sigma_{\mathrm{lg}}} - \sqrt{\sigma_{\mathrm{sg}}})^2}{1 - 0.015\sqrt{\sigma_{\mathrm{lg}}\sigma_{\mathrm{sg}}}}$, where $\beta = 0.000115(\mathrm{m}^2/\mathrm{mJ})^2$ and $\beta_{\mathrm{o}} = 0.0001057(\mathrm{m}^2/\mathrm{mJ})^2$. These given correlations have been compared against each other for some materials and the relative agreement has been reported [29]. The solid surface tensions has a key impact on the behavior of triple line while the liquid-gas surface tension is supposed to be fixed in a certain range, such as the applications of nanofluids in printing conductive wires. The radius of triple line was observed to expand towards the gas phase as the solid surface tensions increases [14].

In general, the characteristics of the substrate, the force balance at the triple line (see Figure 1a, c) and the gravity are the main factors influencing the behavior of triple line of bubbles and droplets. The behavior of triple line can be studied using either the droplet or the bubble method. In the case of droplets, the gravity has a positive impact on the spreading of the triple line, in favour of the reduction of contact angle. As an evidence of that, the behavior of triple line would change tremendously with varying droplet volumes [27-28]. The droplet contact angle can not be a unique criterion to measure the wettability, or the effects of nanoparticles. Similarly it has been clearly observed that the droplet contact angle varies under different gravitational accelerations based on the parabolic flight experiments [36] and drop tower tests [37]. It has been observed that droplet contact angle increases as the effect of gravity decreases. As the gravitational acceleration decreases to zero, the droplet shape gradually changes to a spherical cap. The droplet contact angle under zero gravity has been defined as the asymptotic contact angle, θ_{S}, [7, 27]. The asymptotic contact angle is only dependent on the interactions between gas, liquid and solid at the triple line, and it is a unique criterion to measure the surface wettability or the effects of nanoparticles on surface wettability. The asymptotic contact angle can be obtained experimentally and theoretically. Recently, a new analytical expression has been developed, $r_d \sin\theta_e = \left[\frac{3V}{\pi(2+\cos\theta_s)(1-\cos\theta_s)^2}\right]^{1/3} \sin^2\theta_s$, to calculate the asymptotic contact angle, θ_s, [7, 27], where r_d and V are the radius of the triple line and the droplet volume respectively. Using the asymptotic contact angle, the solid surface tensions can be calculated by having liquid-gas surface tension and the modified form of the Young equation, $\sigma_{lg}\cos\theta_s = \sigma_{sg} - \sigma_{sl}$ [7], which describes the force balance between liquid-gas and solid surface tensions under zero gravity condition.

Another approach has been employed to explain the variation of droplet contact angle with volume, based on the concept of line tension, which has a significant role on adjusting the effect of droplet size on contact angle. In this method, the Young-equation has been modified as, $\frac{\sigma}{r_d} + \sigma_{lg}\cos\theta_e = \sigma_{sg} - \sigma_{sl}$, by considering the effect of line tension, σ. The value of line tension has been obtained experimentally [26, 38] and theoretically [39, 40]. The line tension operates to expand the length of triple line when it is negative and vice versa [38]. Most probably, the line tension would be zero in no-gravity condition, since the droplet contact angle, liquid-gas and solid surface tensions are constant while the radius of triple line would change by volume. It has been reported that (a) the line tension decreases as the wettability increases and likely vanishes at supper wetting conditions [41], (b) the line tension is a function of liquid material [41, 42, 43, 44], and (c) the determination of line tension is still involved with large uncertainties, including both the magnitude and the sign of the line tension [26, 45]. The accurate measurement of line tension is difficult due to a number of issues, including (a) the value of line tension is small, (b) the lack of accurate measurement, (c) the possible contamination in triple line, (d) the lack of accurate modelling, and (e) the effective parameters on line tension is not well recognized yet. So, further studies are needed to provide a better understanding of line tension and the parameters that affect its magnitude and sign. Most of existing studies have been focused on obtaining the value and sign of line tension theoretically and experimentally while it is equally important to understand that how effective is the line tension on different phenomena such as cavitation, boiling, bubble formation and etc. It is also essential to understand the effects of gas phase, solid phase, system pressure and temperature, and the presence of surfactant and nanoparticles on the line tension.

On the cases where the effect of gravity is strong enough to dominate the behavior of triple line based on the droplet method [12], the bubble formation method with very low gas flow rate could be an alternative approach to investigate the behaviour of triple line [11]. For the bubble formation method, the gravity acts as a buoyancy force and pushes the bubble upwards, so the triple line can move more freely with less restriction. As a result, the effects of nanoparticles can be observed much easily. For instance, the pinning behavior of the triple line inside a gold nanofluid has been observed, for the first time, by using the bubble growth method (see Figure 2) [9]. The pinning behavior of the triple line affects subsequently the dynamics of triple line, and the bubble growth and departure process [12].

The characteristics of solid surface [46] such as the homogeneity, roughness and material [47] of substrate have been observed to influence the triple line [48-52] and contact angle hysteresis [24, 53] significantly. The effect of surface roughness on equilibrium contact angle has been considered by Wenzel and Cassie-Baxter equations [48-51]. The conditions of its validity [54], the uncertainties of the estimation [55-56] and the use of correct form of these equations have been discussed in details in reference [57].

The behavior of gas-liquid interface and triple line have been discussed under both stationary conditions, considering surface tension and gravity forces [26-27, 135], and dynamic conditions by modelling appropriately the momentum and moment of momentum balances at the interphase. The details of interfacial transport phenomena can be seen in reference [135]. Many existing investigations are concerned about the effects of the substrate, liquid-gas-solid materials and gravity on the behavior of triple line. However, the effects of roughness, the interactions of gas-liquid-solid at the triple line, the modelling of force balance at the triple line, and the prediction of dynamics of triple line are still challenging and no exact expression exists to consider all these factors at the same time. As a result, the accurate prediction of fluid flow is not possible yet at the vicinity of triple line where gas, liquid and solid meat each other. The modelling of dynamics of triple line would enable us to predict the evolution of bubble formation [11], drop impact [47], initiation of nucleation and boiling heat transfer [17-18] phenomena.

3. Effect of nanoparticles on the behavior of triple line

The affinity of liquids for solid substrates is referred to the wettability of the liquid [25]. Liquids with weak affinities for a solid substrate will collect themselves into spherical shape while those with high affinities for the solid surface will form films to maximize the liquid-solid contact area. For a given droplet volume, the droplet contact angle decreases with the expansion of radius of triple line. The behavior of triple line such as the radius of triple line and contact angle depends on the force balance between liquid-gas and solid surface tensions at the triple line (see Figure 1). Nanoparticles have significant roles on liquid-gas [4-6], solid surface tensions [7] and the force balance at the triple line, affecting its equilibrium and dynamic behaviors [9-10].

It was revealed that the substrate, the concentration and size of bismuth telluride nanoparticles (2.5 nm, 10.4 nm) have great influences on the behavior of triple line. The droplet contact angle was found to increase with the nanoparticle concentration for a given droplet volume. As the nanofluid concentration increased further, the droplet contact angle started decreasing. In contrast to the contact angle, the liquid-gas surface tension of bismuth telluride nanofluid showed an opposite trend [4]. More than 50% reduction in the liquid-gas surface tension was observed for a 2.5 nm bismuth telluride nanofluid. The accumulation and assembly of nanoparticles at the liquid-gas interface was assumed to be responsible for the dependence of liquid-gas surface tension on the nanoparticle concentration. More nanoparticles were driven to the liquid-gas interface region as the concentration of bismuth telluride nanoparticles increased in the bulk liquid. The nanoparticles were bound at the interface [58]. The liquid-gas surface tension continued to decrease due to the electrostatic repulsion and a lower surface energy of the effective interface containing nanoparticle-water, nanoparticle-air and air-water surfaces compared with the original air-water interface. The smaller nanoparticles were observed to be more effective in modifying the behavior of the triple line [4]. The influence of nanoparticles on the liquid-gas surface tension was shown to be dependent on particle materials. For example, the effect of aluminum and alumina nanoparticles on the liquid-gas surface tension [5-6] were found to be negligible or weak.

In addition, different triple line dynamics were observed in the presence of nanoparticles. For example, the evaporation and spreading of aluminum-ethanol nanofluid on a hydrophobic Teflon-AF coated substrate showed that nanoparticles at the vicinity of the triple line could enhance the wetting speed even at low particle concentrations [5], i.e. smaller than 1 % by weight. In another study, the evaporation and dewetting behavior of ethanol-titanium oxide nanofluid droplet on top of PTFE (1 μm thick PTFE layer on silicon wafer substrate) were investigated [20]. The triple line was shown to display a stick-slip behavior while continuous movement of the triple line was observed for the evaporation of pure ethanol droplet on PTFE. The stick-slip behavior of the triple line was attributed to the deposited nanoparticles or the increase of viscosity in the triple region due to high local nanoparticle concentrations. In a separated study, the evaporating droplets containing nanoparticles were studied theoretically based on the lubrication theory, by deriving a system of equations that govern the film thickness and concentration of nanoparticles [21].

The effect of particle size on the pinning behavior of evaporating droplets (5 μl droplet volume and 0.5 v% concentration nanofluid) was investigated [59], using 2 nm Au, 30 nm CuO, 11 nm and 47 nm Al_2O_3 nanoparticles. The particle size was observed to have more effects on the dryout stain pattern than the temperature of the heating surface. The smaller particles resulted in a relatively wider edge accumulation and more uniform central deposition, whereas larger nanoparticles produced a narrower and greater deposition of particles at the edge. The scenario is similar to the dried coffee droplets, where the dispersed solids were observed to migrate to the edge of the droplet, forming a solid ring. The strong liquid evaporation in the triple region would draw liquid from the interior as a result of the capillary flow, which resulted in an outward flow that carried dispersed particles to the edge of the triple line. It was also observed that the pattern and the thickness of the deposited nanoparticles could be controlled by the speed of the evaporation [60-61].

Clearly the deposition and subsequent forming nanoparticle layers is a key factor controlling the behavior of triple line. It has been shown that the number of layers of nanoparticles (i.e., thickness) decreased in a stepwise pattern towards the triple line edge (see Figure 1b). The pattern of nanoparticle distribution at the triple line was influenced by many factors including nanoparticles materials and morphology, particle concentration, nanoparticle surface charge, solid-liquid-gas materials and film depth in the triple region [62-63]. In one study, the rate of spreading of the nanofluid film was shown to be a function of the nanoparticle concentration and the oil drop volume. It was observed that the speed of the inner contact line increased with nanoparticle concentration and decreased with the reduction of drop volume, which is associated with an increase in the capillary pressure [137]. A few theoretical studies have been conducted to explain the dynamics of the triple line in the presence of nanoparticles [138]. It has been shown theoretically that nanoparticles could spread the triple line to a distance of 20-50 times of the particle diameter through a structural disjoining pressure due to the self-ordering of particles in a confined wedge [64]. However, the structural disjoining force only becomes significant at relatively high particle concentrations, i.e. over 20 v%. The layering phenomenon has demonstrated in details in reference [140]. Obviously, the distribution of nanoparticles in the triple line region has an important role in controlling the behavior of triple line and the gas-liquid-solid interactions.

Many of the reported studies were concerned about the effects of the concentration and characteristics of nanoparticles on the layering phenomenon, disjoining pressure, distribution of nanoparticles in triple region, liquid-gas and solid surface tensions. Most of these studies were attempted to explain the effects of nanoparticles on the behavior of triple line in one way or another, but none of them could explain satisfactorily why and how. In order to understand how nanoparticles can be effective, it is essential to understand the detailed interactions of nanoparticles in the liquid, and their interactions with the solid and gaseous phases. While most of these studies were based on the droplet method, the influence of nanoparticles on the behaviour of triple lines and the dynamics of bubbles have been recently studied. Certain nanoparticles have been found to modify significantly the triple line and bubble dynamics, which cannot be described by the classical Young equation, as reviewed below.

4. Dynamics of bubble growth

The formation of bubbles has significant roles in chemical engineering, chemical process industry, petrochemical industry, mineral processing, multiphase flow and boiling heat transfer phenomenon. A large number of experiential and numerical work have been conducted, and a number of influencing factors have been illustrated. The majority of existing studies on the bubble formation have been focused on the effects of the substrate and the diameter of the orifice [15, 74, 80, 82-83, 88-90], volume of gas chamber [89-90, 69-77], gas flow rate [74, 88-90], materials and wettability [74, 88, 75-77], and detailed dynamics of triple line and bubble growth [13-14], as briefly reviewed below.

In most of these applications, bubble departure volume is an important factor that is dependent on the dynamics of triple line and the bubble growth and bubble departure process. Most of the bubble studies have been conducted on either needles or capillary tubes [11-13] and very few studies have used substrate nozzles [13-14, 65, 66]. For substrate nozzles, the radius of triple line is not restricted and can be expanded freely, whereas the radius of triple line on needle nozzles is limited to the outer edge of the needles. Recently, experimental investigations have been conducted to study the behavior of the triple line, bubble growth and bubble departure inside water, silver, gold and alumina nanofluids from stainless steel orifices. It has been observed that nanoparticles play a significant role on the behavior of triple line and consequently they have a great potential to modify the dynamics of bubble growth and departure process [9, 11-12, 14]. A similar experiment has been conducted to study bubble growth inside de-ionized water from 0.5 mm, 0.12 mm and 0.054 mm diameter orifices made by Plexiglas. In this experiment, air was injected using a syringe pump into liquid [66]. As the syringe pump operated in stepwise modes and could not produce a constant and uniform gas flow without a volume chamber. For both cases, the Young-Laplace equation with conventional method could not predict the bubble shapes. To solve the issue, the curve fitting method was employed to predict the bubble shape by dividing the bubble in two parts, i.e., bubble cap as a spherical cap and the main body as a circle. A similar technique was used to define the equation of circumference, passing through the generic point and its neighbouring points [67]. In another attempt, fitting an elliptic equation was used to solve the Young-Laplace equation and to predict the bubble shape [68]. It is clear that the prediction of bubble shape is still challenging and more studies are required.

The dynamics of bubble growth also depend on the chamber volume and the uniformity of the gas flow rate. In the case of large chamber volumes, the possible fluctuation of gas pressure could be damped and the mode of gas flow rate into the chamber and bubble would not be the same. For instance, syringe pumps need a chamber to damp the fluctuations in gas pressure as they operate in a stepwise mode. As chamber volume increases, the fluid flows more smoothly and steadily into the bubble. Large chamber volumes are recommended for systems with high pressure fluctuations [69]. The dependency of dynamics of bubble growth to chamber volume was observed to decrease as the radius of chamber approaches to that of the orifice [70]. The departure bubble volume was found to be independent of the chamber volume when its value and the gas flow rates were small [71-72]. Similarly, the departure bubble volume was observed to increase with the capacitance number, N_c, and gas flow rate at $N_c \prec 25$, where $N_c = 4V_c g\rho_l / \pi D_o^2\, p_h$, with V_c the chamber volume, D_o the orifice diameter and p_h the hydrostatic pressure. For $N_c \succ 25$ the bubble volume was independent of gas flow rate [73].

The variation of gas pressure with time has been measured by locating a pressure sensor between the pump and the orifice. It was observed the gas pressure increased to the maximum at the very beginning of bubble growth and then reduced continuously until the departure point [67]. At the maximum gas pressure, the buoyancy and hydrostatic forces were negligible, since the bubble size was so small. The downward component of surface tension force, $2\sigma_{lg} r_d \pi \sin\theta_o$, is nearly identical with the upward Laplace pressure force, $\dfrac{2\sigma_{lg}}{R_o}\pi r_d^2$, at the apex when bubble volume was small (see equation 5). In fact, the difference between gas and liquid pressures at the apex depends on the radius of curvature at apex, R_0 . At t=0 the liquid-gas interface nearly is flat, thus the radius of curvature at the apex is very big, therefore the Laplace pressure and gas pressure are very small. Similarly, the normal component of surface tension force is small because contact angle is very big. As long as the buoyancy force is negligible, bubble shape grows spherically and the radius of curvature decreases with increasing of bubble volume. Consequently, the Laplace pressure and gas pressure keep increasing. As the buoyancy force starts becoming effective, the bubble begins to be lifted upward and the radius of curvature at apex starts increasing, therefore the Laplace pressure and gas pressure keep decreasing monotonically to the departure point. It has been also reported that the volume of departure increases with orifice diameter for given conditions [74, 66-67]. The Laplace pressure and hydrostatic forces are small at the departure point, and the main effective forces are buoyancy and normal component of surface tension (see equation 5). The buoyancy force and departure volume are nearly proportional to the normal component of the surface tension.

The material and wettability of nozzles were found to have strong effects on the dynamics of bubble growth and bubble departure volume [75-65]. Surface wettability was observed to have the most important influence on bubble size by varying the surface energy of the substrate with controlled deposition of an ultra-thin layer of a plasma polymer [74]. Similar results were obtained by solving the Young-Laplace equation to predict the bubble volume on top of Brass and Teflon substrates for two modes of bubble volume evolution, i.e. the formation at the orifice rim (hydrophilic surface) and the spreading of the bubble base (hydrophobic surface) [65]. It was also reported that the air bubble volume inside water increased more than half as the equilibrium contact angle increased from 68^o to 110^o [75-77]. It was demonstrated that the liquid sometimes moved into the nozzle during the waiting period, because of high surface wettability. As a result, it affected the dynamics of bubble growth and the departure bubble volume. The movement of liquid into the nozzle depends on the nozzle size, wall wettability, gas flow rate, waiting time and gas pressure [78]. It was observed that (a) the bubble departure volume from Teflon tubes with hydrophobic wall was smaller than that from glass tubes with hydrophilic wall, (b) the bubble expansion started sooner from glass tubes, (c) the triple line expanded on Teflon tubes while the triple line always held at the edge of glass tubes, and (d) the liquid incursion into the tubes occurred only for glass tubes [78]. Since the glass tube had higher wettability, the liquid could go into the tube. As a result, the motion of the gas-liquid interface started from the inside of the tubes. Therefore, it had higher Laplace pressure as the radius of curvature of liquid-gas interface inside the glass tube was smaller. So, the gas pressure was lower from the glass tube at the beginning of the bubble formation. That's why the bubble expansion was started sooner and more gas could penetrate into the liquid and produce bigger bubbles. For the given conditions, the liquid could not go into the Teflon tubes due to its hydrophobic surface, so the radius of curvature of liquid-gas interface was higher from Teflon tubes at the beginning of bubble formation.

The liquid viscosity affects the viscous force and apparently it would change the dynamics of bubble growth and departure volume. The effect of viscosity on bubble size is very difficult to detect directly, because as the working fluid varies, many other properties such as the liquid-gas surface tension, solid surface tensions changes, which affects the behaviour of triple line and bubble departure volume. The effect of viscosity could not be isolated alone, which might be one of the reasons responsible for the contradictions on the effect of liquid viscosity. In the literature, it was reported that the departure bubble size (a) increased with liquid viscosity [79-80], (b) had a very weak connection with the viscosity [81], (c) was independent of liquid viscosity [82-84, 71] and (d) was independent of the liquid viscosity for low viscosities while at higher viscosities, the departure bubble size increased with viscosity, but at small flow rates [85].

It should be noted that the effect of liquid-gas surface tension could be different in the top and bottom sides of a bubble. For instance, in the bottom part of bubble close to the orifice, the bubble surface is pulled toward the orifice. Consequently it pushes and holds the bubble on the substrate, delaying bubble departure. On the other hand, the top part of the bubble keeps stretching and generating new surface. The top part of bubble is normally a spherical cap and usually expand relatively faster while the liquid-gas surface tension is comparatively lower or the gas flow rate is fairly higher. The effects of gas flow rate and surface tension on the bubble departure volume has been the subject of some debates for pure fluids and nanofluids. It has been reported that at relatively low gas flow rates, the bubble volume increased with the increase of the surface tension, radius of orifice and was independent of gas flow rate. Though the bubble volume remained fairly independent of the flow rate, the bubble frequency increased as the gas flow rate increased gradually [74]. For high gas flow rates, however, the bubble volume became proportional to the gas flow rate and independent of surface tension [72]. Either viscous or inertia forces determined the bubble volume departure [86]. When gas flow rate was relatively slow, the effect of dynamic gas pressure was negligible, and the bubble departure volume was proportional to the normal component of surface tension. For high gas flow rates, the effects of normal component of surface tension could be negligible comparing with dynamic gas pressure, viscous and inertial forces against bubble expansion. Besides, for a given time, gas has more chance to penetrate into liquid, as gas flow rate increases.

The radius of the orifice is another important factor affecting bubble formation. The radius of the orifice not only will change the departure volume but also it will modify the waiting, bubble formation and total bubble formation times. Here the waiting time is the duration between the end of the previous bubble departure and the beginning of the rapid formation of the current bubble. The bubble formation time starts from the beginning of the rapid formation of the bubble and ends at the departure point. The total bubble formation time is summation of the waiting and bubble formation times. For a given condition, the total bubble formation period increases with the nozzle diameter, so the bubble frequency decreases. In fact, for a given gas flow rate, bubble departure volume increases with the increase of nozzle diameter, so the bubble frequency should be decreased. However, the waiting and bubble formation times do not show a monotonic trend with the nozzle diameter (see Figure 3) [11]. This is due to the inter-play between the capillary pressure and gas dynamic pressure. The gas dynamic pressure for a given gas flow rate is proportional to $1/r^4$ while the capillary pressure is proportional to $1/r$. As the radius of nozzle decreases, the effect of dynamic pressure increases faster than the capillary pressure, therefore the waiting time for smaller nozzle (r= 0.055 mm) is lower. Once the radius of the nozzle increases to 0.255 mm, the capillary pressure decreases; but the reduction of the dynamic pressure is more and consequently the waiting time increases. For the biggest nozzle size (0.42 mm), the effects of capillary pressure and dynamic pressure are not significant and waiting time decreases again. Similar behavior was observed for different gas flow rates.

The effect of partial confinement on the dynamics of bubble growth and departure volume has been studied numerically and experimentally by injecting gas through an orifice into cylindrical tube or conical space, filled with viscous liquid. The departure bubble volume was affected by the angle of the cone or the radius of the cylinder. The results confirmed that the departure volume of the vertically elongated bubbles were significantly larger than those of the round bubbles, generated in the absence of walls, where the radius of cylindrical was smaller than six times of the radius of the orifice, or when the angle of the cone was smaller than 30^{o} [87]. As bubble grew inside a cylinder or a cone filled with liquid, the surrounded liquid moves downward and eventually, the liquid filled the gap after the bubble departure.

As the angle of the cone or the radius of cylinder decreases, the downward liquid flow becomes more difficult especially in viscous fluids which produces an extra force against bubble expansion in the vertical direction. Therefore a higher buoyancy forces or bigger bubble volume was required to depart the bubble from the orifice. The buoyancy, viscous drag and viscous friction with the wall have a key role on dynamics of bubble growth and bubble departure volume.

As shortly reviewed above, there are many factors that can influence bubble formation significantly, with still many existing contradictory results. Clearly more investigations are still needed to reveal clearly the effect of gas flow rate, inertial force, size and geometry of orifices, dynamics of bubble growth and departure process, inside homogenous liquids and nanofluids. The modelling of bubble growth, especially under high non-equilibrium conditions still presents as a big challenge, as reviewed below.

4.1 Prediction of bubble shape

A number of methods have been developed to predict bubble shape, which can be generally categorized as the mechanical approach or the fluid mechanics approach. The former approach is focused on the mechanical balance across the interface, and a classical example is the Young-Laplace method, which as reviewed above, has the problems in modeling bubbles under high non-equilibrium conditions. The latter method deals with the momentum equations from both fluids with applied boundary conditions across the interface. The fluid approach ranges from semi-analytical and simplified analytical methods to full numerical simulation based on computational fluid dynamics (CFD) approaches. A short review is developed below to explain the nature, weakness and references of these methods for further elaborations.

The Young-Laplace equation, $\Delta p = \left(\frac{1}{R_1} + \frac{1}{R_2} \right)$, represents a mechanical equilibrium condition between two fluids separated by an interface. Where R_1 and R_2 are the radii of curvatures, i.e. R_1 is the radius of curvature describing the latitude as it rotates and R_2 is the radius of curvature in a vertical section, describing the longitude as it rotates. Traditionally, the Young-Laplace equation has been solved to predict the droplet [4, 7, 10, 26-27, 106-111] and bubble [11-12, 27, 112-113] shapes. The Young-Laplace equation can predict the liquid-gas interface where (a) gas and liquid phases are in equilibrium, (b) gas flow rate is steady and relatively slow enough to neglect the liquid-gas shear stress and the variation of momentum and (c) bubble is not stretched upward and effect of viscosity is negligible. Under these conditions, the Young-Laplace equation is able to predict the bubble shape, knowing only two bubble parameters among the bubble height, radius of triple line, contact angle and bubble volume. The Young-Laplace equation has been observed to be able to predict the bubble shape from needle nozzles (0.11-0.84 mm internal diameters), for nominal air flow rates of 0.015-0.7 ml/min. A good agreement has been observed between experimental data and prediction of the Young-Laplace equation [11-15]. Similarly, it has been observed that the Young-Laplace equation was not able to predict the bubble shape in the departure period [11-16] when the bubble was stretched upward or while gas flow rate was relatively high [141].

From the fluid mechanics consideration, the Rayleigh-Plesset equation is widely applied as a simplified approach predict bubble shapes. The Rayleigh-Plesset equation can be derived from the integration of the Navier-Stokes equation or differentiation with respect to radius of bubble from balance between the kinetic energy in the liquid and the potential energy in the gas [128]. The Rayleigh-Plesset equation is able to predict the variation of bubble radius as a function of time, however it is only limited to the spherical bubbles and the effect of the surface wettability is neglected. Many examples have show that the Rayleigh-Plesset equation can be applied successfully to predict the dynamics of bubble growth while it was restricted to the spherical shape[118-121, 136].Some attempts have been made to modify the Rayleigh-Plesset equation to predict the bubble radius oscillations in response to the imposed fluctuating pressure field [137], but with limited success.

Extending to more complicated bubble conditions, a number of numerical methods have been developed to predict bubble shapes. Examples include the prediction of the bubble [114-117, 122-123] and impact droplet [124-125] shapes by solving numerically the momentum and continuity equations. Many of these simulations were based on commercial codes such as FLUENT and CFX, where the Young equation was used to incorporate the effect of surface wettability in order to predict the liquid-gas interface in the vicinity of a substrate. However the Young equation is not valid for the most of cases[27], including axisymmetric bubbles and droplets. The accuracy and the reliability of any numerical approach for bubble prediction are down to the proper modelling of the dynamics and of the triple line and the fluid around it, whose understanding is essentially insufficient at the moment. The situation becomes worsen when the speed of triple line is high, in fluctuation, or the characteristics of substrate is far from ideal in terms of the surface roughness and homogeneity..

The suitability of bubble shape prediction by the Young-Laplace equation has been examined by several numerical simulations based on the volume of fluid (VOF) and level-set (LS) methods [114-115], and good agreement has been reported. . For example, a coupled LS and VOF method was used to predict the bubble growth, bubble detachment and bubble rise for low and medium air flow rates. The bubble dynamics was modelled by various approaches, including the algebraic compressive scheme of VOF (Open FOAM), geometric VOF (ANSYS-Fluent V13), LS (TransAT) and geometric coupled VOF with LS (CLSVOF) (ANSYS-Fluent V13) method, and compared with experimental data from an orifice of 1.6 mm in diameter under flow rate of 50, 100, 150 and 200 ml/h. The results illustrated that (a) the level of accuracy of predictions of all four methods were decreased as the bubble grew larger , (b) the LS method gave better bubble shape prediction compared with other methods while the VOF-com method was less accurate [116]. It was also observed that the static contact angle had a significant influence on the prediction of bubble growth. Increasing the contact angle above a threshold value could increase the bubble departure volume and departure time by allowing the triple line to expand away from the orifice rim. The threshold contact angle was observed to be nearly identical with the minimum contact angle during the bubble growth [117]. The coupled LS and VOF method [115] also showed the importance of the gravity in affecting bubble dynamics, which is consistent with the general trend of the Young-Laplace prediction.

.

4.2 Analytical expressions

From the mechanical equilibrium approach, the analytical expressions have been developed initially to predict the bubble departure volume which was mainly based on the force balance analysis under different assumptions; these expressions can be used for different purposes. Under a quasi-steady state condition, a relationship [91-94] was developed between bubble departure volume, V , and gas flow rate, Q , as

$$V = N \frac{Q^{6/5}}{g^{3/5}} \tag{1}$$

g was the gravitational acceleration and N was a constant, N=1.378. It was assumed that the upward motion was determined by the buoyancy force and mass acceleration of the fluid, surrounding the bubble. The constant N was modified, 1.138, later on. Equation (1) was also achieved by two-stage bubble growth model (expansion and detachment stages) [95]. In the first stage, the bubble was assumed to expand and remain on top of the orifice while downward forces were dominant. The beginning of detachment stage was assumed to start from the end of expansion stage, where the bubble was started to move away from the orifice to the departure point. In case of two stage model, the constant was N=0.976. The bubble shape was assumed to be spherical for both models. The first stage of two-stage model was modified [96] by assuming that the bubble was expanding in a hemispherical shape. The bubble was switched to the second stage by transforming to a detaching spheroid as it reached a certain size. The maximum volume of the first stage was calculated by writing the force balance between reactive forces on the plate and forces on the expanding surface such as pressure due to expansion and hydrostatic pressure. The second stage was considered to be similar to that of the previous model [94]. As a result, equation (1) was again obtained with a different constant of N=1.09. Obviously, the bubble shape cannot be spherical at the presence of gravity, unless the bubble size is so small. The small bubbles remain suspended inside the liquid, since buoyancy force is negligible and they need an external force to move upward after detachment [97]. Besides, the effect of surface wettability has not been considered in equation (1) while behavior of triple line has significant effects on dynamics of bubble growth and bubble volume departure [13-14, 57-59, 74, 88]. Equation (1) can only be considered as a very primary approach to predict the bubble departure.

Subsequently, the force balance has been employed [98] between forces due to buoyancy, surface tension and change in momentum of the liquid to derive the following equation

$$\rho_l gV - [\rho_l g(\delta - C_1 R_o) - \frac{2\sigma_{lg}}{R_o}]\pi r_d^2 - 2\pi r_d \sigma_{lg} \sin\theta_o = (m_a + \rho_g V)a \qquad (2)$$

where the coefficient C_1 is an empirical constant, related to the shape of the curved upper surface, m_a is the added mass due to the expansion and the rise of bubble, and a is the upward acceleration of the bubble. The second term of equation (2) contains the corrections for the negative buoyancy of the cylinder, or hydrostatic term, $[\rho_l g(\delta - C_1 R_o)]\pi r_d^2$, and it is included an empirical constant which is made this equation very complicated unnecessarily. The magnitude of hydrostatic term is very small compare to the values of Laplace pressure, normal component of liquid-gas surface tension and buoyancy forces [11, 15]. The accuracy of equation (2) and credibility of coefficient C_1 need to be investigated more precisely.

Equation (3) has been developed, considering the effects of buoyancy, drag, inertial and surface tension forces where D, d, ρ_l, μ_l and α respectively are bubble diameter, nozzle diameter, liquid density, liquid viscosity and dimensionless inertial parameter ($0.5 \prec \alpha \prec 11/16$).

$$\frac{\pi}{3} D^3 \rho_l g = (\frac{81C_d}{16} + 9\alpha)\frac{\rho_l Q^2}{\pi D^2} + \pi d\sigma_{lg} \rightarrow C_d = \frac{16\mu_l \pi D^3}{3\rho_l dDQ} + 1 \quad (3)$$

Similarly, another correlation [99] has been developed, assuming that, the bubble shape is spherical throughout the bubble growth, under constant gas flow rate, $Q = \frac{dV}{dt}$, as

$$\begin{aligned}(\rho_l - \rho_g)gV + \frac{\rho_g Q^2}{(\pi/4)d^2} = \\ \pi d\sigma_{lg} + (\rho_g - \xi_1\rho_l)\frac{d}{dt}(V\frac{ds}{dt}) + \frac{1}{2}\rho_l \frac{\pi}{4} D^2 C_D (\frac{ds}{dt} - v_w)\left|\frac{ds}{dt} - v_w\right|\end{aligned} \quad (4)$$

Equation (4) is the combination of buoyancy, $(\rho_l - \rho_g)gV$, gas momentum flux, $\frac{\rho_g Q^2}{(\pi/4)d^2}$, surface tension, $\pi d\sigma_{lg}$, added mass inertia, $(\rho_g - \xi_1\rho_l)\frac{d}{dt}(V\frac{ds}{dt})$, and drag, $\frac{1}{2}\rho_l \frac{\pi}{4} D^2 C_D (\frac{ds}{dt} - v_w)\left|\frac{ds}{dt} - v_w\right|$, forces, where $\xi_1, \frac{ds}{dt}, C_D$ and v_w respectively are added mass coefficient defined as 11/16, bubble center velocity, drag force coefficient [100] and average impressed velocity [101] of the previous bubble wake. Equations (3-4) have not been considered, the effect of wettability while it has been shown that behavior of wettability has a significant role on dynamics of bubble growth. Besides, the primary assumption of spherical bubble growth for both correlations is far from reality and cannot be practical. The next expressions have been developed by writing force balance on a slice of a bubble between z and z+dz, along the vertical and horizontal axes, two different differential equations have been derived. By taking integral from these differential equations, the following analytical expressions have been obtained

$$(\rho_l - \rho_g)gV + \frac{2\sigma_{lg}}{R_o}\pi r_d^2 - (\rho_l - \rho_g)g\delta\pi r_d^2 - 2\sigma_{lg} r_d \pi \sin\theta_o = 0 \quad (5)$$

$$\sigma_{lg} S - [\frac{2\sigma_{lg}}{R_o} A + (\rho_g - \rho_l)g\bar{z}A] + 2r_d \sigma_{lg}\cos\theta_o = 0 \quad (6)$$

Both equations 5 [15] and 6 [141] were mathematically proved to be the exact analytical solution of the Young-Laplace equation. In fact, equation (5) is a force balance between downward hydrostatic, $(\rho_l - \rho_g)g\delta\pi r_d^2$, downward component of surface tension, $2\sigma_{lg} r_d \pi \sin\theta_o$, upward buoyancy, $(\rho_l - \rho_g)gV$ and upward Laplace pressure, $\frac{2\sigma_{lg}}{R_o}\pi r_d^2$, and equation (6) is a force balance in a horizontal axis between surface tension force at the perimeter of bubble, $\sigma_{lg}S$, hydrostatic force, $[\frac{2\sigma_{lg}}{R_o}A + (\rho_g - \rho_l)g\bar{z}A]$, and horizontal component of surface tension force at the vicinity of triple line, $2r_d\sigma_{lg}\cos\theta_o$. Practically, equation (6) proves that the Young equation is not valid for bubbles. In fact, equation (6) can be applied instead of the Young equation in CFD calculations to reduce the level of uncertainty and errors. Similar to equation (6), another analytical expression was developed for droplets, which is the exact analytical solution of the Young-Laplace equation [141]. Later on, equation (5) has been modified by adding the effect of inertial force against of bubble expansion in vertical direction [13] and gas flow rate [15]. Another expression is developed by considering the force balance between upward partial buoyancy, upward contact pressure, $\pi r_d^2(p_g - p_t)$, downward component of surface tension forces, where p_t is liquid pressure at the bubble apex. Partial buoyancy force has been defined as an upward force, assuming the triple line is pinned at the rim of nozzle during the bubble growth. It is assumed the net upward force only acts on the partial volume of bubble which is equal with total bubble volume minus volume of a cylindrical column with radius of triple line and height of bubble [67]. By adding the first and third terms of equation (5), the partial buoyancy force can be obtained.

Similar force balance method has been also used to develop an expression to predict the bubble size at a nucleation site. The force balance between the surface tension, the unsteady drag, the pressure, the gravity and quasi-steady forces, acting on a bubble at a nucleation site, can be seen in references [129]. In addition, a few other theoretical expressions [102-105] have been developed based on the force balance method.

The gas flow rate has crucial roles on the dynamics of bubble growth and bubble departure. Considering the effect of gas flow rate, several correlations and analytical expressions have been developed, including equations (1, 3-4). For spherical bubbles, the effect of gas flow rate on pressure difference between liquid and gas phases has developed [131] by considering viscosity and liquid-gas surface tension as follows

$$p_g = p_l + \frac{\mu Q}{\pi r_s^3} + \frac{2\bar{\sigma}_{lg}}{r_s} \tag{7}$$

where r_s, μ, $\bar{\sigma}_{lg}$ are radius of spherical bubble, shear viscosity and mean surface tension respectively. A simultaneous consideration of viscosity and surface tension is the advantage of equation (7). Recently, equation (5) has developed [15] by considering the effect of gas flow rate as follows

$$(\rho_l - \rho_g)gV + \frac{2\sigma_{lg}}{R_o}\pi r_d^2 - (\rho_l - \rho_g)g\delta\pi r_d^2 - 2\sigma_{lg} r_d \pi \sin\theta_o + \frac{\rho_g Q^2}{2\pi r_d^2} = 0 \tag{10}$$

Properly modelling of the effect of gas flow rate is essential, because the gas flow rate has important influences on the pressure difference between the gas and liquid phases, the geometry of gas-liquid interface and dynamics of bubble growth and departure process.

For a proper modelling, the oscillation of gas-liquid interface is the key parameter that has to be taken into the consideration. The oscillation of gas-liquid interface before bubble detachment has been investigated in reference [13] and it has been considered after bubble detachment by several others [133-134]. Similarly, the oscillation of spherical gas-liquid interface has been explored [132] for drops in gases by neglecting the effect of viscosity,

In spite of long time working on theoretical approaches, it has not been made much of progress. Most of existing analytical expressions are valid in certain conditions and they are not accurate out of those conditions. For bubbles under high non-equilibrium conditions, such as before the departure and during the oscillation period, the validity of these analytical expressions requires careful examination. The next generation of analytical expressions has to consider the effective parameters such as gas flow rate, buoyancy, Laplace pressure, hydrostatic, gas and liquid inertial, drag and surface tension forces as well as gas flow rate and viscosity, especially under non-equilibrium conditions.

The remaining part of the paper will perform an experimental investigation on the effect of nanoparticles on the triple line and bubble dynamics, develop a new method to calculate the pressure difference between gas and liquid phases along the bubble perimeter, and compare the results in between.

5. Experimental setup

In the bubble formation experiment, air is injected into water and different nanofluids through stainless steel substrate nozzles to observe the effects of nanoparticles on the dynamics of triple line and bubble growth. The schematics of experimental setup is shown in

Figure 4. Two different stainless steel substrate nozzles with diameters of 0.4 mm and 0.51 mm and a stainless steel needle with internal diameter of 0.51 mm were submerged into a transparent square-sized glass container with a 20 mm by 20 mm base and 72 mm height. The substrate nozzles were polished to reduce the roughness (with average value of the peaks and valleys, $R_a = 0.021\mu m$, and the largest difference from peak-to-valley, $R_Z = 0.03\mu m$) and were large enough to allow the triple line to expand freely. The glass container was filled with deionized water or nanofluid to a height of 20 mm and was open to the atmosphere. The gas flow was supplied by compressed air in a cylinder, connected to a gas flow controller (model F-200CV-002 of Bronkhorst) through a pressure reduction valve. Nominal gas flow rates in range of 0.1-0.7 ml/min were used with an accuracy of $\pm 0.5\%$. The dynamics of triple line and bubble growth were captured by a high speed camera (Photosonics Phantom V4.3, 1200 frames/sec) equipped with an optical microscope head (10X Navitar Macro zoom 7000). The resolution of the camera was 5 μm per pixel. The profile of bubbles were obtained from the captured images by fast camera equipped with a microscope during the bubble growth from 0.4 mm substrate nozzles, inside water and gold nanofluids with three different concentrations of 1E-4, 5E-4, and 10E-4 by weight. The captured images were stored in the computer for more analysis.

Well-defined gold nanoparticles, with a narrow size distribution averaged at 5 nm for gold was dispersed into deionized water without any surfactant (see Figure 5). A drop of gold nanofluid was left on top of a stainless steel surface to dry slowly. The dried nanofluid droplet was analyzed by an Energy Dispersive x-Ray Spectroscopy (EDX), which confirmed the purity of the nanoparticles. The Drop Shape Analysis System (KRUSS, DSA 100) was employed to obtain the surface tension of water and gold nanofluid. The surface tension of pure water, 1E-4, 5E-4, and 10E-4 gold nanofluids were 0.07238 ± 0.0041, 0.06753 ± 0.005, 0.0615 ± 0.0052 and 0.0591 ± 0.0055 N/m Respectively.

6. Analytical force balance

In this study, the force balance is applied on a slice of a bubble along the vertical axis to find an analytical expression between the radius of curvature at upper apex, R_o, and other bubble parameters. A schematic view of effective forces on a slice of a bubble, extending between z and $z + dz$ along the vertical axis is shown in Figure 6. The force balance equation is written along the vertical direction on a slice of a bubble as

$$\sum F_z = -dF_b(z) - F_p(z+dz) + F_p(z) - F_\sigma(z)\sin\theta + F_\sigma(z+dz)\sin(\theta + d\theta) = 0 \tag{7}$$

F_b, F_p and F_σ are respectively forces due to buoyancy, pressure and liquid-gas surface tension. Equation (7) can be simplified as

$$dF_b(z) + d[F_p(z) - F_\sigma(z)\sin\theta] = 0 \tag{8}$$

The individual elements of equation (8) include the buoyancy force,

$$dF_b = (\rho_l - \rho_g)g\pi r^2 dz \tag{9}$$

the force due to pressure difference

$$F_p(z) = [\Delta p(z)]\pi r^2 \tag{10}$$

and the force due to the liquid-gas surface tension

$$F_\sigma(z) = \sigma_{lg} 2\pi r \tag{11}$$

where $\Delta p(z)$ is the pressure difference between gas, $p_g(z)$, and liquid phases, $p_l(z)$. The gas and liquid pressures as a function of z are given by

$$p_g(z) = \frac{2\sigma_{lg}}{R_o} + \rho_g gz + p_o \tag{12}$$

$$p_l(z) = \rho_l gz + p_o \tag{13}$$

where $\frac{2\sigma_{lg}}{R_o}$ is the pressure difference at the bubble apex and R_o is the radius of curvature at the upper apex. $\rho_g gz$ is hydrostatic gas pressure, $\rho_l gz$ is hydrostatic liquid pressure and p_o is the pressure at the apex due to hydrostatic pressure or anything else. Interestingly, p_o has no role on pressure difference at the interface. $\Delta p(z) = p_g(z) - p_l(z)$ is given by

$$\Delta p(z) = \frac{2\sigma_{lg}}{R_o} - (\rho_l - \rho_g)gz \tag{14}$$

By substituting equations (9-14), equation (8) can be modified as

$$(\rho_l - \rho_g)g\pi r^2 dz + d[(\frac{2\sigma_{lg}}{R_o} - (\rho_l - \rho_g)gz)\pi r^2 - 2\sigma_{lg} r\pi\sin\theta) = 0 \tag{15}$$

Equation (15) can be rewritten as

$$\begin{aligned}(\rho_l - \rho_g)gr^2 + \frac{4\sigma_{lg}}{R_o} r\frac{dr}{dz} - g(\rho_l - \rho_g)gz(r^2 + 2rz\frac{dr}{dz}) \\ - 2\sigma_{lg}(\frac{dr}{dz}\sin\theta + r\frac{d\sin\theta}{d\theta}\frac{d\theta}{ds}\frac{ds}{dz}] = 0\end{aligned} \tag{16}$$

Knowing $\tan\theta = \frac{dz}{dr}$ and $dz = ds\sin\theta$, equation (16) can be transformed to the Young-Laplace equation, $\frac{d\theta}{ds} = \frac{2}{R_o} - \frac{gz}{\sigma_{lg}}(\rho_l - \rho_g) - \frac{\sin\theta}{r}$. In fact, it proves mathematically that the solution of equation (15) is identical with the exact analytical solution of the Young-Laplace equation.

By taking integral from zero to z_m (see Figure 6), where $z_m = r_m$, equation (15) can be solved as

$$(\rho_l - \rho_g)gV_m + (\frac{2\sigma_{lg}}{R_o} - (\rho_l - \rho_g)gz_m)\pi r_m^2 - 2\sigma_{lg}r_m\pi = 0 \tag{17}$$

Equation (17) is an exact analytical solution of the Young-Laplace equation. The experimental evidence shows that the upper part of bubble is nearly hemisphere and V_m can be obtained with a good approximation by

$$V_m = \frac{2}{3}\pi r_m^3 \tag{18}$$

Substituting equation (18) into equation (17), a new analytical expression is derived to express the radius of curvature at the apex as

$$R_o = (\frac{(\rho_l - \rho_g)gr_m}{6\sigma_{lg}} + \frac{1}{r_m})^{-1} \tag{19}$$

Equation (19) gives a new analytical expression to predict the radius of curvature at the upper apex by knowing maximum radius of bubble, r_m, (see Figure 6). For given experimental data, the radius of curvature, R_o, is predicted by equation (19) and the Young-Laplace equation. A good agreement is observed between these two.

6.1 Prediction of bubble shape

The Young-Laplace equation has been used to predict the bubble [11-12, 15, 89, 130] and droplet [7, 27, 130] shapes. The Young-Laplace equation can be derived by considering the force balance at the liquid-gas interface. By writing force balance along the $\vec{n}$-direction (see Figure 7), the following equation is obtained

$$dF_n = 2\sin(\frac{d\alpha}{2})dF_1 + 2\sin(\frac{d\theta}{2})dF_2 \approx \sigma_{lg}(R_1 d\alpha d\theta + R_2 d\theta d\alpha) \tag{20}$$

$$dF_n = \Delta p dA_n = (p_g - p_l)dA_n \tag{21}$$

By equating equations 20 and 21, and assuming that the static pressure and surface tension forces are only effective elements, the Young-Laplace equation can be obtained as

$$\Delta p = (\frac{1}{R_1} + \frac{1}{R_2})\sigma_{lg} \tag{22}$$

The Young-Laplace equation demonstrates a mechanical equilibrium between two fluids, separated by an interface, and gives the pressure difference across the liquid-gas interface as a function of the product of the curvature multiplied by the liquid-gas surface tension. R_1, and R_2 are the radii of the curvature at the liquid-gas interface, where R_1 is the radius of curvature describing the latitude as it rotates and R_2 is the radius of curvature in a vertical section, describing the longitude as it rotates. The centres of R_1 and R_2 are on the same line, vertical to the liquid-gas interface, but different location (see Figure 7). The formulation of the Young-Laplace equation can be seen in reference [130]. Obviously, the Young-Laplace equation can be applied under a quasi-steady state condition, where the static pressure and surface tension forces are only effective elements and there is an equilibrium condition between gas and liquid at the interface.

The Young-Laplace equation is modified by introducing an extra force along the $\vec{n}$-direction (a) when the equilibrium between gas and liquid is relatively weak during the bubble fluctuation, (b) the while bubble is stretched upward, in departure period or (c) when gas flow rate is relatively high and the shear stress is not negligible. Employing extra force, equation (21) can be modified as

$$\Delta p R_1 R_2 d\alpha d\theta - \sigma_{lg}(R_1 d\alpha d\theta + R_2 d\theta d\alpha) \pm dF_{ex} = 0 \tag{23}$$

Simplifying equation (23), the following equation is obtained

$$\Delta p \pm p_{ex} = \sigma_{lg}(\frac{1}{R_1} + \frac{1}{R_2}) \tag{24}$$

p_{ex} is positive while the interface is pushed toward the liquid phase in $\vec{n}$-direction and vice versa. Any extra forces on the liquid-gas interface area, dA, have two components of tangential and vertical. In case of axisymmetric bubbles, the tangential components cancel each other and normal components divided by area can be represented as p_{ex} in $\vec{n}$-direction.

The radii of curvature (see Figure 7) are

$$R_1 = ds / d\theta, \text{ and } R_2 = r / \sin\theta \tag{25}$$

θ, r and s are respectively the bubble contact angle, radius of the bubble and length of bubble perimeter at the location of z (see Figure 8). Considering equations 14 and 25, equation (24) for bubbles becomes

$$\frac{d\theta}{ds} = \frac{2}{R_o} - \frac{gz}{\sigma_{lg}}(\rho_l - \rho_g) - \frac{\sin\theta}{r} + \frac{p_{ex}}{\sigma_{lg}} \tag{26}$$

The sign of p_{ex} is assumed to be positive in equation (26), however the real sign can be obtained when equation (26) is solved. If p_{ex} is zero, then equation (26) reforms to the Young-Laplace equation and can be written as

$$\frac{d\theta}{ds} = \frac{2}{R_o} - \frac{gz}{\sigma_{lg}}(\rho_l - \rho_g) - \frac{\sin\theta}{r} \tag{27}$$

The radius of curvature at the upper apex, R_o, can be calculated from equation (19), knowing maximum radius of bubble, r_m. To obtain the axisymmetric bubble shape, equation (26) can be solved with following system of ordinary differential equations

$$\frac{dr}{ds} = \cos\theta \tag{28}$$

$$\frac{dz}{ds} = \sin\theta \tag{29}$$

$$\frac{dV}{ds} = \pi r^2 \sin\theta \tag{30}$$

where V is bubble volume. Equations 26 and 27 avoid the singularity problem at the bubble apex, since

$$\left.\frac{\sin\theta}{r}\right|_{s=0} = \frac{1}{R_o} \tag{31}$$

In case of nanofluids, the liquid-gas surface tension, σ_{lg}, need to be changed to the liquid-gas surface tension of nanofluids, σ_{lgn}.

In order to raise the accuracy of the prediction of bubble shape, the bubble is divided into k parts (k=1:N) and the system of ordinary differential equations (26, 28-30) along with equation (19) is solved for each individual part separately to obtain the extra pressure, p_{ex}, and bubble shape simultaneously by knowing the radius, r, and height, z, at the end of the each part (see Figure 8). The first part, k=1, starts from the apex (point A) with given initial boundary conditions, $r(0) = z(0) = \theta(0) = V(0) = 0$. Because of the continuity of the bubble shape, the second part, k=2, starts from the end of the first part. So the initial boundary conditions of the second part, k=2, such as radius, r, height, z, contact angle, θ, and volume, V, are identical with those at the end of the first part, k=1. Similarly the system of ordinary differential equations (26, 28-30) along with equation (19) can be solved separately for the rest of the parts. The accuracy of the prediction of bubble shape increases with the number of parts, N, or the reduction of distance between two nodes, Δs, for each individual part. In fact, the effects of inertia force and viscosity decrease with respect to liquid-gas surface tension as the distance between the two nodes, Δs, decreases (see Figure 8) and consequently, the validity and accuracy of prediction of the Young-Laplace equation for the bubble shape increase. The case of N=1 and $p_{ex} = 0$ corresponds to the conventional method of applying the Young-Laplace equation to predict the bubble shape while there is an equilibrium between gas and liquid phases, shear stress and inertial force are negligible and bubble is not stretched upward. The experimental evidences have been confirmed that the system of differential equations (27-30) was valid for the given conditions.

The system of ordinary differential equations (26, 28-30) along with equation (19) is solved to predict the upper and lower parts of bubble shape. For the given conditions, a reliable agreement is observed between the prediction of bubble shape and the experimental data by dividing bubble shape in two parts (N=2). The first part is started from upper apex and ended at the lateral apex. Similarly the second part is started from lateral apex and ended at the triple line. The quality of bubble prediction increases with the number of parts, N.

7. Results and discussion

The force balance was employed on a slice of bubble, extending between z and $z + dz$, in vertical axis, to obtain an analytical equation (17) among the bubble parameters such as bubble volume, maximum radius of bubble and radius of curvature at apex. Combining equations 17 and 18, an analytical expression (19) was developed to predict the radius of curvature at apex, R_o, as a function of maximum radius of bubble, r_m. In addition, the Young-Laplace equation (27) along with equations (28-30) was solved for the upper part of bubble to obtain the radius of curvature at apex, R_o. The upper part of bubble was started from upper apex and ended at the lateral apex. Figure 9 compares the radius of curvature at apex, R_o, predicted by the Young-Laplace equation and the analytical expression (19), inside water and gold nanofluid with different concentrations, i.e. 1e-4 w, 5e-4 w and 10e-4 w, from a 0.4 mm stainless steel substrate nozzle under a nominal air flow rate of 0.7 ml/min. The mean absolute parentage error between the radius of curvature, predicted by the Young-Laplace equation and analytical expression (19) is 0.00451, for all given experimental data. Experimental evidence demonstrates that equation (19) is accurate enough to predict the radius of curvature at apex, R_o, knowing the maximum radius of bubble, r_m.

Figure 10 shows the prediction of bubble shape inside gold nanofluid (1e-4 w) from 0.4 mm stainless steel substrate nozzle under a nominal air flow rate of 0.7 ml/min. The bubble shape is divided to 26 parts, i.e, N=26. The system of ordinary differential equations (26, 28-30) along with equation (19) is solved for each individual part to predict the bubble shape. The prediction of bubble shape was compared with experimental data and parentage of absolute average error was calculated. The mean absolute parentage error was 1.2 and 0.5 while N was respectively for N=2 and 26. In fact, the mean absolute parentage error decreased with number of parts, k.

The system of ordinary differential equations (26, 28-30) along with equation (19) is solved for each individual part separately to obtain the extra pressure, p_{ex}, across the liquid-gas interface, along the bubble perimeter. The variation of p_{ex} with s can be seen in Figure 11 when (a) bubble stops growing upward and start moving downward at t=604.109 ms, (b) starts growing upward again at t=607.442 ms and (c) in the middle of these two points at t=605.775 ms where bubble accelerating downward and the equilibrium between gas and liquid is weaker. p_{ex} was observed to fluctuate across the liquid-gas interface which implies that the liquid-gas interface oscillated along the bubble perimeter from one point to another. The amplitude of pressure oscillation at t=607.442 ms was relatively higher, because the equilibrium between gas and liquid was weaker. The quality of Figure 11 can be increased with the number of experimental points, i.e. by using a higher speed camera with higher resolution.

In case of bubble growth from needle nozzle, the value of p_{ex} is negligible and no oscillation is observed along the liquid-gas interface. The bubble fluctuation and oscillation of pressure difference between gas and liquid are only observed for bubble growth from substrate nozzle. This indicates that the oscillation of pressure difference between gas and liquid is attributed to the bubble fluctuation.

To investigate the oscillation of bubble in bubble growth period, the air was injected into water to produce bubble from stainless steel substrate and needle nozzles. The internal diameter of stainless steel substrate and needle nozzles was 0.51 mm. No oscillation was observed while bubble was forming from needle nozzle. For the same conditions, the bubble was observed to oscillate from a substrate nozzle. The Young-Laplace equation (27) along with equations (28-30) was solved (N=1) to predict the bubble shape inside water from stainless steel needle nozzle by knowing the radius of triple line and bubble height. Having bubble shape, characteristics of bubble such as volume and contact angle can be obtained.

Knowing characteristics of bubble, the variation of effective forces on bubble were calculated in bubble growth period. Figure 12 demonstrates the variation of main forces on bubbles with time inside water from stainless steel needle and substrate nozzles, for nominal gas flow rate of 0.7 ml/min. The internal diameter of stainless steel substrate and needle nozzles was 0.51 mm.

The main forces are due to the Laplace pressure (upward), $\frac{2\sigma_{lg}}{R_o}\pi r_d^2$, buoyancy (upward), $(\rho_l - \rho_g)gV$, vertical component of the surface tension (downward), $2\sigma_{lg} r_d \pi \sin\theta_o$, and inertial (downward), $\frac{d(MU)}{dt} = -(\frac{11}{16}\rho_l + \rho_g)[V\frac{d^2\delta}{dt^2} + \frac{dV}{dt}\frac{d\delta}{dt}]$ [13]. The inertial force was reached to its maximum from stainless steel substrate and needle nozzles respectively in 1.1% and 3.9% of their bubble formation time. In addition, the maximum of inertial force from substrate nozzle was 2.8 times bigger than that from needle nozzle. The inertial force was raised quickly to its maximum and pushed the bubble downward. The bubble was begun to oscillate under the effect of high downward inertial force, since air was compressible fluid. The fluctuation of bubble from substrate nozzle was related to high inertial force, effective in a short period of time. For the same conditions, the bubble fluctuation was not observed from needle nozzle, since the maximum inertial force was effective in a longer time with a lower value.

This study also investigated the effects of nanoparticles on the behavior of triple line. Suspended nanoparticles have considerable influence on variation of the liquid-gas [4] and solid surface tensions [7]. As a result they are able to change the force balance at the triple line. Figure 13 demonstrates the variation of radius of triple line with time inside water, gold (1E-4 w), silver (1E-4 w) and alumina (0.37E-4 w) nanofluids from 0.4 mm stainless steel substrate, for 0.7 ml/min nominal air gas flow rate. It clearly illustrates how gold, silver and alumina nanofluids affect the behavior of triple line differently. Nanoparticles affect the liquid-gas and solid surface tensions and they consequently change the force balance at the triple line and as a result the contact angle and radius of triple line might alter. It is clear that the gold nanoparticles increased the pinning behavior of triple line and reduced the radius of triple line significantly, which was attributed to variation of nanofluid solid surface tensions. It has been observed that radius of triple line increased toward the liquid phase as solid surface tensions, $\sigma_{sg} - \sigma_{sl}$, decreased [14]. Among water, gold and silver nanofluids, gold nanofluid had the maximum solid surface tensions and the minimum radius of triple line while the silver nanofluid had the minimum solid surface tensions and maximum radius of triple line. The resistance force against the expansion of triple line inside silver nanofluid was observed to be weaker. Consequently, the silver nanofluids had the maximum radius of triple line.

For the given droplet volume, the water contact angle was smaller than that of alumina nanofluid which means the solid surface tensions of alumina nanofluid is lower than that of water. Since the liquid-gas surface tension of water and alumina nanofluid are relatively similar at the low concentration of 0.001 v%, the solid surface tensions has an important role on the variation of droplet contact angle. The triple line expands more toward the gas phase, with solid surface tensions.

The material of nanoparticles has a significant role on the behavior of triple line inside nanofluids. In fact, the behavior of triple line such as variation of contact angle and radius of triple line depends on the base liquid, gas, solid, concentration and characteristics of nanoparticles. These parameters affect the liquid-gas and solid surface tensions. Consequently they change the force balance at the triple line and modify the contact angle and radius of triple line.

Figures 14 and 15 demonstrate the variation of bubble contact angle and radius of triple line with time inside water and gold nanofluids with three different concentrations (1E-4, 5E-4, and 10E-4 by weight). Different concentrations of nanofluid change the waiting time, bubble formation time and total bubble formation period as well as bubble frequency. The waiting and bubble formation times decreased with the concentration of gold nanoparticle, which might be attributed to the reduction of liquid-gas surface tension with concentration of gold nanofluid. The waiting time is proportional to the capillary pressure and capillary pressure is proportional with liquid-gas surface tension. Consequently the waiting time and total bubble formation period decreased with decreasing liquid-gas surface tension.

The radius of triple line was observed not to distort much with the concentration of gold nanoparticle, which might imply that force balance at the triple line was not influenced much by the concentration of gold nanofluid. The bubble volume departure was observed to decrease with reduction of liquid-gas surface tension. As liquid-gas surface tension reduces, downward surface tension force, $-2\sigma_{lg} r_d \pi \sin\theta_o$, decreases; so bubble requires less buoyancy force, $(\rho_l - \rho_g) gV$, to departure which would result in a reduction of bubble departure volume [82-83, 126]. However a few other studies reported that there is no effect of surface tension on bubble departure volume [80, 91], whereas others showed that the bubble departure volume increased with the decrease of surface tension [127]. |There are difficulties to evaluate the role of liquid-gas surface tension alone, as the bubble departure volume is modulated by many other experimental variables such as orifice diameter, gas-liquid-solid physical properties and gas flow rate.

The variation of bubble contact angle with time inside gold nanofluid (5E-4 w) can be seen in Figure15. At the beginning of bubble growth, bubble volume was very small, $0 \le V \le 9.9933E-10$, $0.5649ms \le t \le 0.5666ms$, so the effect of buoyancy force was negligible, therefore the bubble expanded laterally and contact angle decreased with bubble volume. As bubble volume increased further, $9.9933E-10 \le V \le 6.3437E-9$, $0.5666ms \le t \le 0.5782ms$, the effect of buoyancy force became more effective gradually. As a result, the bubble lifted upward increasingly and the bubble contact angle began to increase and eventually reached to its maximum. In the meantime, the oscillation of bubble initiated and so the bubble contact angle began to decrease at $6.3437E-9 \le V \le 8.2873E-9$, $0.5782ms \le t \le 0.5899ms$. Eventually the bubble contact angle reached to its second minimum. As volume increased further, the bubble contact angle resumed to increase again till the bubble departure point, $8.2873E-9 \le V \le 9.9221E-9$, $0.5899ms \le t \le 0.6066ms$.

8. Conclusions

This work reviews the dynamics of triple line and theoretical modeling of bubble growth and departure process, with a particular focus on the influence of nanoparticles, and advances the field through new experimental and theoretical studies. In a short summary:

i) The presence of gold nanoparticle was found to reduce the bubble waiting and formation times, which might be attributed to the reduction of liquid-gas surface tension due to the presence of gold nanoparticles, and the triple line dynamics was not sensitive to the particle concentrations.

ii) Experimentally no oscillation of liquid-gas interface or bubble fluctuation was observed from the needle nozzle. However for bubble formation from the stainless steel substrate nozzle, the downward inertial force was observed to increase in a short period of time to a high value, resulting in bubble fluctuations.

iii) A theoretical model was developed to raise the accuracy of prediction of bubble shape when the bubble was in non-equilibrium. Different to conventional approach of applying the Young-Laplace equation on the whole bubble, here bubble was divided into the several parts (k=1:N) and the Young-Laplace equation was solved for each part separately, which improved the accuracy of bubble shape prediction. The new method can be applied to many situations such as a) the equilibrium between gas and liquid phases at the interface was weak, b) the bubble was stretched upward in departure period and c) the shear stress between gas and liquid phases was relatively high.

iv) The theoretical model was examined with experimental data and good agreement was observed. Using this method, the pressure difference between gas and liquid phases was calculated during the bubble fluctuation period. The pressure difference was observed to oscillate along the liquid-gas interface, which was attributed to the oscillation of the liquid-gas interface across the bubble.

Nomenclature

A	Bubble cross section area $[m^2]$
g	Acceleration of gravity $[m/s^2]$
R_o	Radius of curvature at apex $[m]$
R_1, R_2	Radius of curvature $[m]$
r_d	Radius of triple line $[m]$
S	Perimeter of bubble cross section $[m]$
V	Bubble Volume $[m^3]$

Greek Symbols

δ	Height of apex $[m]$
θ_o	Bubble contact angle [Deg.]
θ_e	Equilibrium contact angle [Deg.]
θ_s	Asymptotic contact angle [Deg.]
ρ_l	Liquid density $[kg/m^3]$
ρ_g	Gas density $[kg/m^3]$
σ_{lg}	Liquid-gas surface tension $[N/m]$
σ_{sg}	Solid-gas surface tension $[N/m]$
σ_{sl}	Solid-liquid surface tension $[N/m]$

σ_{lgn} Liquid-gas surface tension of nanofluids $[N/m]$

References

[1] Buongiorno J et al, A benchmark study on the thermal conductivity of nanofluids, Journal of Applied Physics, 2009; 106: 0943121.

[2] Vafaei S, Wen, Convective heat transfer of aqueous alumina nanosuspensions in a horizontal mini-channel, Heat and Mass Transfer, 2012; 48: 349.

[3] Godson L, Raja B, Mohan Lal D, Wongwises S, Experimental investigation on the thermal conductivity and viscosity of silver-deionized water nanofluid, Experimental Heat Transfer, 2010; 23: 317.

[4] Vafaei S, Purkayastha A, Jain A, Ramanath G, Borca-Tasciuc T, The effect of nanoparticles on the liquid-gas surface tension of Bi2Te3 nanofluids, Nanotechnology, 2009; 20: 185702.

[5] Sefiane K, Skilling J, MacGillivray J, Contact line motion and dynamic wetting of nanofluid solutions, Advances in Colloid and Interface Science, 2008; 138: 101.

[6] Kim SJ, Bang IC, Buongiorno J, Hu LW, Surface wettability change during pool boiling of nanofluids and its effect on critical heat flux, International Journal of Heat Mass Transfer, 2007; 50: 4105.

[7] Vafaei S, Wen D, Borca-Tasciuc T, Nanofluids surface wettability through asymptotic contact angle, Langmuir, 2011; 27: 2211.

[8] de Gennes PG, Wetting: statics and dynamics, Reviews of Modern Physics, 1985; 57, 827.

[9] Vafaei S, Wen D, The effect of gold nanoparticles on the spreading of triple line, Microfluidics and Nanofluidics, 2010; 8: 843.

[10] Vafaei S, Borca-Tasciuc T, Podowski MZ, Purkayastha A, Ramanath G, Ajayan PM, Effect of nanoparticles on sessile droplet contact angle, Nanotechnology, 2006; 17: 2523.

[11] Vafaei S, Wen D, Bubble formation in a quiescent pool of gold nanoparticle suspension, Advances in Colloid and Interface Science, 2010; 159: 72.

[12] Vafaei S, Wen D, Effect of gold nanoparticles on the dynamics of gas bubbles, Langmuir, 2010; 26: 6902.

[13] Vafaei S, Angeli P, Wen D, Bubble growth rate from stainless steel substrate and needle nozzles, Colloids and Surfaces A: Physicochemical and Engineering Aspects, 2011; 387: 240.

[14] Vafaei S, Wen D, Spreading of triple line and dynamics of bubble growth inside

nanoparticle dispersions on top of a substrate plate, Journal Colloid Interface Science, 2011; 362: 285.

[15] Vafaei S, Borca-Tasciuc T, Wen D, Theoretical and experimental investigation of quasi-steady-state bubble growth on top of submerged stainless steel nozzles, Colloids and Surfaces A: Physicochemical and Engineering Aspects, 2010; 369: 11.

[16] Vafaei S, Wen D, Bubble formation on a submerged micronozzle, Journal of Colloid and Interface Science, 2010; 343: 291.

[17] Vafaei S, Wen D, Critical heat flux (CHF) of subcooled flow boiling of alumina nanofluids in a horizontal microchannel, Journal of Heat Transfer, 2010; 132: 102404.

[18] Vafaei S, Wen D, Flow boiling heat transfer of alumina nanofluids in single microchannels and the roles of nanoparticles, Journal of Nanoparticle Research, 2011; 13: 1063.

[19] Sefiane K, On the role of structural disjoining pressure and contact line pinning in critical heat flux enhancement during boiling of nanofluids, Applied Physics Letters, 2006; 89: 0441061.

[20] Moffat JR, Sefiane K, Shanahan MER, Effect of TiO2 nanoparticles on contact line stick-slip behavior of volatile drops, Journal of Physical Chemistry B, 2009; 113: 8860.

[21] Craster RV, Matar OK, Sefiane K, Pinning, retraction, and terracing of evaporating droplets containing nanoparticles, Langmuir, 2009; 25: 3601.

[22] Sefiane K, Bennacer R, Nanofluids droplets evaporation kinetics and wetting dynamics on rough heated substrates, Advances in Colloid and Interface Science, 2009; 147: 263.

[23] Forrest E, Williamson E, Buongiorno J, Hu LW, Rubner M, Cohen R, Augmentation of nucleate boiling heat transfer and critical heat flux using nanoparticle thin-film coatings, International Journal of Heat and Mass Transfer, 2010; 53: 58.

[24] Kandlikar SG, Steinke ME, Contact angles and interface behavior during rapid evaporation of liquid on a heated surface, International Journal of Heat and Mass Transfer, 2002; 45: 3771.

[25] Carey VP, Liquid-vapor phase-change phenomena, Hemisphere Publishing Corporation, Second edition, 2008.

[26] Neumann AW, Spelt JK, Applied Surface Thermodynamics, M. Dekker, 1996.

[27] Vafaei S, Podowski MZ, Analysis of the relationship between liquid droplet size and contact angle, Advances in Colloid and Interface Science, 2005; 113: 133.

[28] Gaydos J, Neumann AW, The dependence of contact angles on drop size and line

tension, Journal of Colloid and Interface Science, 1987; 120: 76.

[29] Kwok DY, Neumann AW, Contact Angle Measurement and Contact Angle Interpretation, Advances in Colloid and Interface Science, 1999; 81: 167.

[30] Berthelot D, Sur le mélange des gaz. Comptes rendus hebdomadaires des séances de l'Académie des Sciences, 1898: 126: 1703.

[31] Li D, Neumann AW, Reformulation of the equation of state for interfacial tensions, Journal of Colloid Interface Science, 1990; 137: 304.

[32] Kwok DY, Neumann AW, Contact angle interpretation in terms of solid surface tension, Colloids and Surfaces A: Physicochemical and Engineering Aspects, 2000; 161: 31.

[33] Kwok DY, Contact angles and surface energetics, Ph.D. Thesis, University of Toronto, 1998.

[34] Driedger O, Neumann AW, Sell PJ, An Equation of State Approach for Surface Free Energies," Kolloid-Z. Z. Polym, 1965; 201: 52.

[35] Neumann AW, Good RJ, Hope CJ, Sejpal M, An equation-of-state approach to determine surface tensions of low-energy solids from contact angles, Journal of Colloid Interface Science, 1974; 49: 291.

[36] Brutin D, Zhu ZQ, Rahli O, Xie JC, Liu Q, Tadrist L, Sessile Drop in Microgravity: Creation, Contact Angle and Interface, Microgravity Science and Technology, 2009; 21: 67.

[37] Diana A, Castillo M, Brutin D, Steinberg T, Sessile Drop Wettability in Normal and Reduced Gravity, Microgravity Science and Technology, 2012; 24: 195.

[38] Chen P, Susnar SS, Mak C, Amirfazli A, Neumann AW, Lens size dependence of contact angle and the line tension of the dodecane-water-air system, Colloids and Surfaces A: Physicochemical and Engineering Aspects, 1997; 129-130, 45.

[39] Hoorfar H, Amirfazli A, Gaydos JA, Neumann AW, The effect of line tension on the shape of liquid menisci near stripwise heterogeneous walls, Advances in Colloid and Interface Science, 2005; 114–115, 103.

[40] Marmur A, Line Tension and the Intrinsic Contact Angle in Solid-Liquid-Fluid Systems, Journal of Colloid and Interface Science, 1997; 186, 462.

[41] Amirfazli A, Keshavarz A, Zhang L, Neumann AW, Determination of line tension for systems near wetting, Journal of Colloid and Interface Science, 2003; 265, 152.

[42] Amirfazli A, Chatain D, Neumann, AW, Drop size dependence of contact angles for liquid tin on silica surface: line tension and its correlation with solid–liquid interfacial tension, Colloids and Surfaces A: Physicochemical and Engineering Aspects, 1998; 142, 183.

[43] Duncan D, Li D, Gaydos J, Neumann AW, Correlation of Line Tension and Solid-Liquid Interfacial Tension from the Measurement of Drop Size Dependence of Contact Angles, Journal of Colloid and Interface Science, 1995; 169, 256.

[44] Amirfazli A, Kwok DY, Gaydos J, Neumann AW, Line Tension Measurements through Drop Size Dependence of Contact Angle, Journal of Colloid and Interface Science, 1998; 205, 1.

[45] Amirfazli A, Neumann AW, Status of the three-phase line tension, Advances in Colloid and Interface Science, 2004;110, 121.

[46] Gao L, McCarthy TJ, Wetting 101, Langmuir, 2009; 24:14105.

[47] Antonini C, Amirfazli A, Marengo M, Drop impact and wettability: From hydrophilic to superhydrophobic surfaces, Physics of Fluids, 2012; 24: 1021041.

[48] Wenzel RN, Resistance of solid surfaces to wetting by water, Industrial and Engineering Chemistry, 1936; 28: 988.

[49] Cassie ABD, Discussions of the Faraday Society, 1948; 3: 11.

[50] Baxer S, Cassie ABD, Journal of Text. Inst, 1945; 36T: 67.

[51] Cassie ABD, Baxter S, Transactions of the Faraday Society, 1944; 40: 546.

[52] Wolansky G, Marmur A, Apparent contact angles on rough surfaces: the Wenzel equation revisited, Colloids and Surfaces A: Physicochemical and Engineering Aspects, 1999; 156: 381.

[53] Gao L, McCarthy TJ, Contact angle hysteresis explained, Langmuir, 2006; 22: 6234.

[54] Marmur A, Bittoun E, When Wenzel and Cassie Are Right: Reconciling Local and Global Considerations, Langmuir, 2009; 25:1277.

[55] Gao L, McCarthy TJ, How Wenzel and Cassie were wrong, Langmuir, 2007; 23: 3762.

[56] Gao L, McCarthy TJ, An attempt to correct the faulty intuition perpetuated by the Wenzel and Cassie "laws", Langmuir, 2009; 25: 7249.

[57] Milne AJB, Amirfazli A, The Cassie equation: How it is meant to be used, Advances in Colloid and Interface Science, 2012; 170: 48.

[58] Ally J, Kappl M, Butt HJ, Amirfazli A, Detachment force of particles from air-liquid interfaces of films and bubbles, Langmuir, 2010; 26: 18135.

[59] Chon CH, Paik S, Tipton JB, Kihm KD, Effect of nanoparticle sizes and number densities on the evaporation and dryout characteristics for strongly pinned nanofluid droplets, Langmuir, 2007; 23: 2953.

[60] Deegan RD, Bakajin O, Dupont TF,Huber G, Nagel SR, Witten TA, Capillary flow

as the cause of ring stains from dried liquid drops, Nature, 1997; 389: 827.

[61] Deegan RD, Bakajin O, Dupont TF, Huber G, Nagel SR, Witten TA, Contact line deposits in an evaporating drop, Physical Review E 62, 2000; 1: 756.

[62] Wasan DT, Nikolov AD, Spreading of nanofluids on solids, Nature, 2003; 423: 156.

[63] Nikolov A, Kondiparty K, Wasan D, Nanoparticle self-structuring in a nanofluid film spreading on a solid surface, Langmuir, 2010; 26: 7665.

[64] Chengara A, Nikolov D, Wasan DT, Trokhymchuk A, Henderson D, Spreading of nanofluids driven by the structural disjoining pressure gradient, Journal of Colloid and Interface Science, 2004; 280: 192.

[65] Gerlach D, Biswas G, Durst F, Kolobaric V, Quasi-static bubble formation on submerged orifices, International Journal of Heat and Mass Transfer, 2005; 48: 425.

[66] Xie J, Zhu X, Liao Q, Wang H, Ding YD, Dynamics of bubble formation and detachment from an immersed micro-orifice on a plate, International Journal of Heat and Mass Transfer, 2012; 55, 3205.

[67] Bari SD, Robinson AJ, Experimental study of gas injected bubble growth from submerged orifices, Experimental Thermal and Fluid Science, 2013; 44,124.

[68] Hernández-Baltazar E, Gracia-Fadrique J, Elliptic solution to the Young–Laplace differential equation, Journal of Colloid and Interface Science, 2005; 287, 213.

[69] Kulkarni AA, Joshi JB, Bubble formation and bubble rise velocity in gas-liquid systems: a review, Industrial & Engineering Chemistry Research, 2005; 44: 5873.

[70] Hayes WB, Hardly BW, Holland CD, Formation of gas bubbles at submerged orifices, A. I. Ch. E. Journal, 1959; 5: 319.

[71] Hughes RR, Handlos AE, Evans HD, Maycock RL, The formation of bubbles at simple orifices, Chemical Engineering Progress, 1955; 51: 557.

[72] Davidson L, Amick EH, Formation of gas bubbles at horizontal orifices, A. I. Ch. E. Journal, 1956; 2: 337.

[73] Tsuge H, Hibino SI, Bubble formation from an orifice submerged in liquids, Chemical Engineering Communications, 1983; 22, 63.

[74] Lin JN, Banerji SK, Yasuda H, Role of interfacial tension in the formation and the detachment of air bubbles, 1. A single hole on a horizontal plane immersed in water, Langmuir, 1994; 10: 936.

[75] Gnyloskurenko SV, Byakova AV, Raychenko OI, Nakamura T, Influence of wetting conditions on bubble formation at orifice in an inviscid liquid, Transformation of bubble shape and size, Colloids and Surfaces A: Physicochemical and Engineering Aspects, 2003;

218: 73.

[76] Gnyloskurenko SV, Byakova AV, Nakamura T, Raychenko OI, Influence of Wettability on bubble formation in liquid, Journal of Materials Science, 2005; 40: 2437.

[77] Byakova AV, Gnyloskurenko SV, Nakamura T, Raychenko OI, Influence of wetting conditions on bubble formation at orifice in an inviscid liquid: Mechanism of bubble evolution, Colloids and Surfaces A: Physicochemical and Engineering Aspects, 2003; 229: 19.

[78] Zhu X, Liao Q, Wang H, Bao LJ, Xie J, Lin CX, Experimental study of bubble growth and departure at the tip of capillary tubes with various wettabilities in a stagnant liquid, Journal of Superconductivity and Novel Magnetism, 2010; 23, 1141.

[79] Khurana AK; Kumar R, Studies in bubble formation-III, Chemical Engineering Science, 1969; 24, 1711.

[80] Quigley CJ, Johnson AI, Harris BL, Size and mass transfer studies of gas bubbles, Chemical Engineering Symposium Series, 1955; 16: 31.

[81] Vasilev AS, Laws governing the outflow of a jet of gas into a liquid. Theoretical Foundations of Chemical Engineering, 1970; 4, 727.

[82] Datta RL, Napier DH, Newitt DM, The properties and behaviour of gas bubbles formed at a circular orifice, Transactions of the Institution of Chemical Engineers, 1950; 28: 14.

[83] Benzing RL, Myers JE, Low frequency bubble formation at horizontal circular orifices, Industrial and Engineering Chemistry, 1955; 47: 2087.

[84] Kumar R, Kuloor NR, The formation of bubbles and drops, Advances in Chemical Engineering; Academic Press: New York, 1970; 8, 255.

[85] Kim I, Kamotani Y, Ostrach S, Modeling bubble and drop formation in flowing liquids in microgravity, AIChE Journal, 1994; 40, 19.

[86] Snabre P, Magnifotcham F, Formation and rise of a bubble stream in a viscous liquid, The European Physical Journal B, 1998; 4, 369.

[87] Lopez-Villa A, Medina A, Higuera, FJ, Bubble growth by injection of gas into viscous liquids in cylindrical and conical tubes, Physics of Fluids, 2011; 23, 102102.

[88] Corchero G, Medina A, Higuera FJ, Effect of wetting conditions and flow rate on bubble formation at orifices submerged in water, Colloids and Surfaces A: Physicochemical and Engineering Aspects, 2006; 290: 41.

[89] Marmur A, Rubin E, Equilibrium shapes and quasi-static formation of bubbles at submerged orifice, Chemical Engineering Science, 1973; 28: 1455.

[90] Marmur A, Rubin E, A theoretical model for bubble formation at an orifice submerged in an inviscid liquid, Chemical Engineering Science, 1976; 31: 453.

[91] Davidson JF, Schuler BOG, Bubble formation at an orifice in an inviscid liquid, Transactions of the Institution of Chemical Engineers, 1960; 38: 335.

[92] Davidson JF, Schuler BOG, Transactions of the Institution of Chemical Engineers, 1960; 38: 144.

[93] Walters JK, Davidson JF, Fluid Mechanics, 1962; 17: 321.

[94] Davidson JF, Harrison H, Fluidised Particles, Cambridge University Press, Cambridge, 1963.

[95] Kumar R, Kuloor NR, Chemical Technology, 1967; 19: 733.

[96] Wraith AE, Chemical Engineering Science, 1971; 26: 1659.

[97] Zimmerman WB, Tesař V, Bandulasena HCH, Towards energy efficient nanobubble generation with fluidic oscillation, Current Opinion in Colloid Interface Science, 2011; 16, 350.

[98] Mori BK, Baines WD, International Journal of Heat and Mass Transfer, 2001; 44: 771.

[99] L. Zhang, M. Shoji, Aperiodic bubble formation from a submerged orifice, Chemical Engineering Science, 2001; 56, 5371.

[100] Sekoguchi K, Kikai no kenkyu, Two-phase flow, Tokyo: Yokendo Ltd, 1974; 1.234.

[101] Schlichting H, Boundary layer theory, New York: McGraw-Hill, 1960.

[102] McCann DJ, Prince RG, Regimes of bubbling at a submerged orifice, Chemical Engineering Science, 1971; 26: 1505.

[103] Mitrovic J, Bubble detachment criteria, International Journal of Heat Mass Transfer, 1997; 40: 209.

[104] Ramakrishnan S, Kumar R, Kuloor NR, Chemical Engineering Science, 1969; 24: 731.

[105] Satyanarayan A, Kumar R, Kuloor NR, Chemical Engineering Science, 1969; 24: 749.

[106] Padday JF, The profiles of axially symmetric minisci, Phil Trans Roy Soc London Ser A. Math Phys Sci, 1971; 269: 265.

[107] del Rio OI, Neumann AW, Axisymmetric drop shape analysis: Computational methods for the measurement of interfacial properties from the shape and dimensions of pendant and sessile drops, Journal of Colloid and Interface Science, 1997; 196: 136.

[108] Vafaei S, Podowski MZ, The modeling of liquid droplet shape on horizontal and inclined surfaces, 5th ICMF, Yokohama, Japan, May 30-June 4, 2004.

[109] Bateni A , Susnar SS, Amirfazli A, Neumann AW, A novel methodology to study shape and surface tension of drops in electric fields, Microgravity Science and Technology, 2005; 16: 153.

[110] Bateni A , Susnar SS, Amirfazli A, Neumann AW, Development of a new methodology to study drop shape and surface tension in electric fields, Langmuir, 2004; 20: 7589.

[111] Bateni A, Laughton S, Tavana H, Susnar SS, Amirfazli A, Neumann AW, Effect of electric fields on contact angle and surface tension of drops, Journal of Colloid and Interface Science, 2005; 283: 215.

[112] Longuet-Higgins MS, Kerman BR, Lunde K, Release of air bubbles from an underwater nozzle, Journal of Fluid Mechanics, 1991; 230: 365.

[113] Chen Y, Groll M, Dynamics and shape of bubbles on heating surfaces: A simulation study, International Journal of Heat and Mass Transfer, 2006; 49: 1115.

[114] Gerlach D, Tomar G, Biswas G, Durst F, Comparson of volume of fluid methods for surface tension-dominant two phase flows, International Journal of Heat and Mass Transfer, 2006; 49: 740.

[115] Chakraborty I, Ray B, Biswas G, Durst F, Sharma A, Ghoshdastidar PS, Computational investigation on bubble detachment from submerged orifice in quiescent liquid under normal and reduced gravity, Physics of Fluids, 2009; 21: 621031.

[116] Albadawi A, Donoghue DB, Robinson AJ, Murray DB, Delaure´ YMC, On the analysis of bubble growth and detachment at low capillary and Bond numbers using volume of fluid and level set methods, Chemical Engineering Science, 2013; 90, 77.

[117] Albadawi A, Donoghue DB, Robinson AJ, Murray DB, Delaure´ YMC, Influence of surface tension implementation in volume of fluid and coupled volume of fluid with level set methods for bubble growth and detachment, International Journal of Multiphase Flow, 2013; 53, 11.

[118] Pinczewski WV, The formation and growth of bubbles at a submerged orifice, Chemical Engineering Science, 1981; 36, 405.

[119] Di Marco P, Grassi W, Memoli G, Takamasa T, Tomiyama A, Hosokawa S, Influence of electric field on single gas-bubble growth and detachment in microgravity, International Journal of Multiphase Flow, 2003; 29, 559.

[120] Loubiere K, H-ebrard G, Bubble formation from a #exible hole submerged in an inviscid liquid, Chemical Engineering Science, 2003; 58, 135.

[121] Das AK, Das PK, Saha P, Formation of bubbles at submerged orifices – Experimental investigation and theoretical prediction, Experimental Thermal and Fluid Science, 2011; 35, 618.

[122] Gerlach D, Alleborn N, Buwa VV, Durst F, Numerical simulation of periodic bubble formation at a submerged orifice with constant gas flow rate, Chemical Engineering Science, 2007; 62, 2109.

[123] Buwa VV, Gerlach D, Durst F, Schlucker E, Numerical simulations of bubble formation on submerged orifices: Period-1 and period-2 bubbling regimes, Chemical Engineering Science, 2007; 62, 7119.

[124] Pasandideh-Fard M, Qiao YM, Chandra S, Mostaghimi J, Capillary effects during droplet impact on a solid surface, Physics of Fluids, 1996; 8, 650.

[125] Sprittles JE, Shikhmurzaev YD, The Dynamics of liquid drops and their interaction with solids of varying wettabilites, Physics of Fluids, 2012; 24, 082001.

[126] Coppock PD, Meiklejohn GT, The behaviour of gas bubbles in relation to mass transfer, Transactions of the Institution of Chemical Engineers, 1951: 29: 75.

[127] Martin M, Montes FJ, Galan MA, On the influence of the liquid physical properties on bubble volumes and generation times, Chemical Engineering Science, 2006; 61: 5196.

[128] T.G. Leighton, Derivation of the Rayleigh-Plesset equation in terms of volume, ISVR Technical Report No 308, 2007.

[129] Ishii M, Hibiki T, Thermo-fluid dynamics of two-phase flow, Springer, Berlin, 2006.

[130] Hartland S, Hartley RW, Axisymmetric fluid-liquid interfaces, Elsevier, New York, 1976.

[131] Edwards DA, Brenner H, Wasan DT, Interfacial transport processes and rheology, Butterworth-Heinemann, Boston, 1991.

[132] Temkin S, Suspension Acoustics, Cambridge Univ. Pr., Cambridge, 2005.

[133] Brenner MP, Lohse D, Dupont TF, Bubble Shape Oscillations and the Onset of Sonoluminescence, Physical Review Letters,1998; 80, 3668.

[134] Akhatov S, Vakhitova NK, Galeyeva GY, Nigmatulin RI, Khismatullin DB, Weak oscillations of a gas bubble in a spherical volume of compressible liquid, Journal of Applied Mathematics and Mechanics, 1997; 61, 921.

[135] Slattery JC, Sagis L, Oh ES, Interfacial transport phenomena, Springer, 2007.

[136] Brennen CE, Cavitation and Bubble Dynamics, Oxford Univ. Pr., Oxford, 1995.

[137] Liu KL, Kondiparty K, Nikolov AD, Wasan D, Dynamics Spreading of Nanofluids on Solids Part I - Experimental, Langmuir, 2012, 28, 14618.

[138] Liu KL, Kondiparty K, Nikolov AD, Wasan D, Dynamics Spreading of Nanofluids on Solids Part II - Modelling, Langmuir, 2012, 28, 16274.

[140] Nikolov AD, Wasan D, Wetting–dewetting films: The role of structural forces, Advances in Colloid and Interface Science 206 (2014) 207.

[141] Vafaei S, Theoretical and experimental investigations of dynamics of bubble growth and triple line, The Canadian Journal of Chemical Engineering, accepted.

Figures

Figure 1. Schematic of forces at the bubble/droplet triple line.

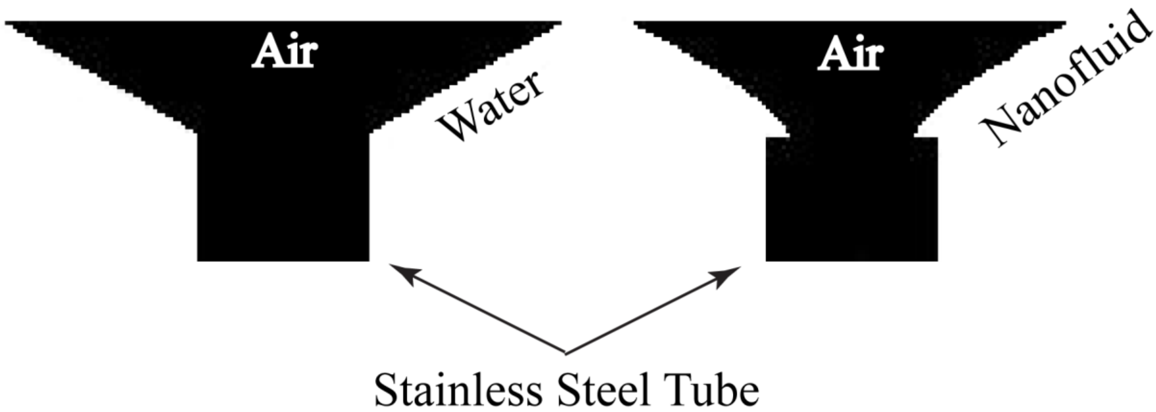

Figure 2. Comparison of the radius of contact lines of gas bubbles on top of a stainless steel tube (outside radius 105 μm) between water (left) and 1E-4 w gold/water nanofluid (right) at bubble volume of 2.73 μl . Gas flow rate is 0.48 ml/min [10].

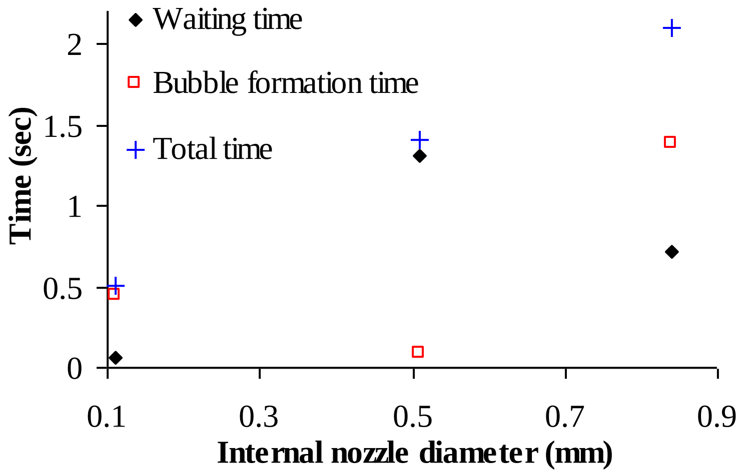

Figure 3. Variation of waiting, formation, and total times with internal diameter of needle nozzle for 0.48 ml/min gas flow rate [14].

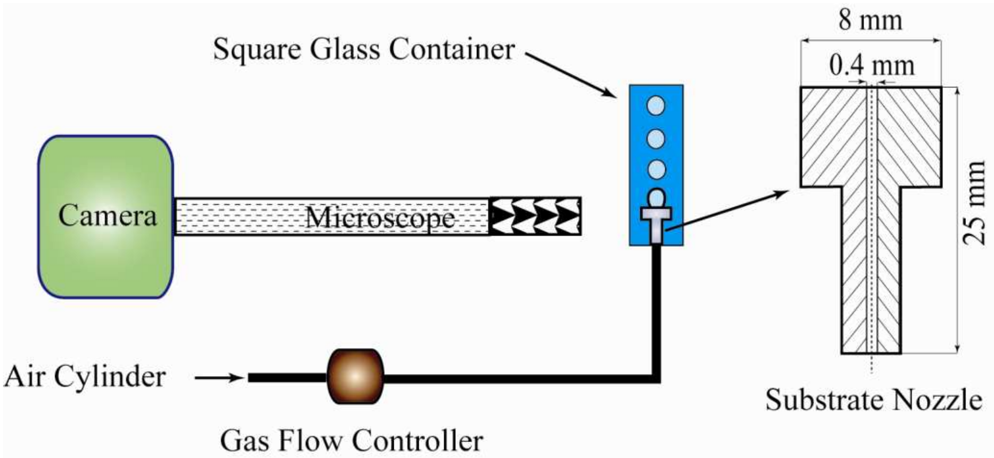

Figure 4. Schematic of the experimental setup.

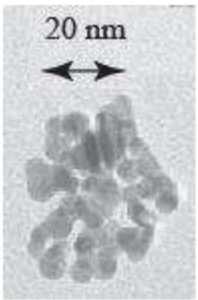

Figure 5. Transmission electron microscopy (TEM) pictures of gold nanoparticles.

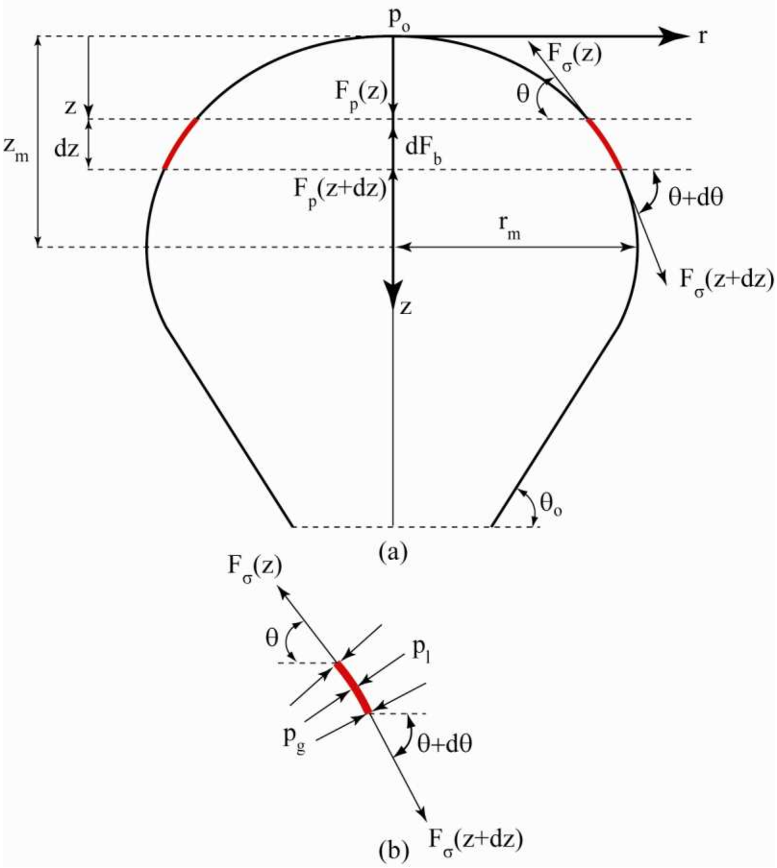

Figure 6. Schematic of effective forces on a slice of axisymmetric bubble, extending between z and $z + dz$, along the vertical axis.

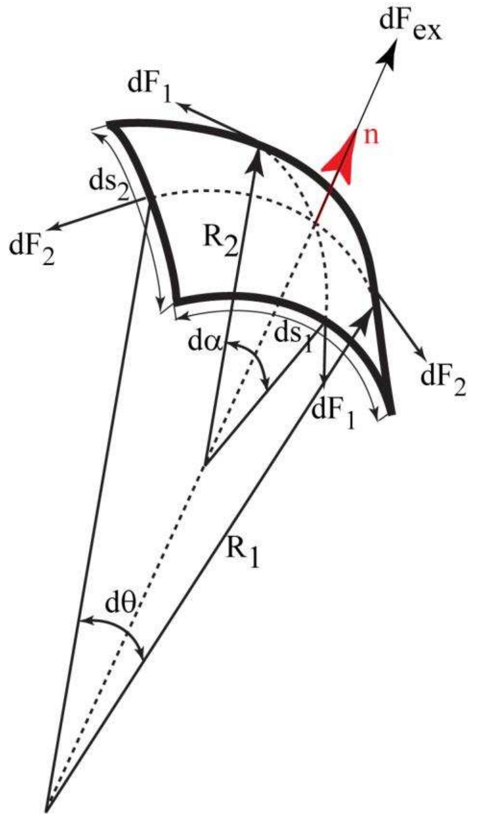

Figure 7. Schematic of geometry and surface forces of three dimensional liquid-gas interface. Gas is inner phase and liquid is outer phase.

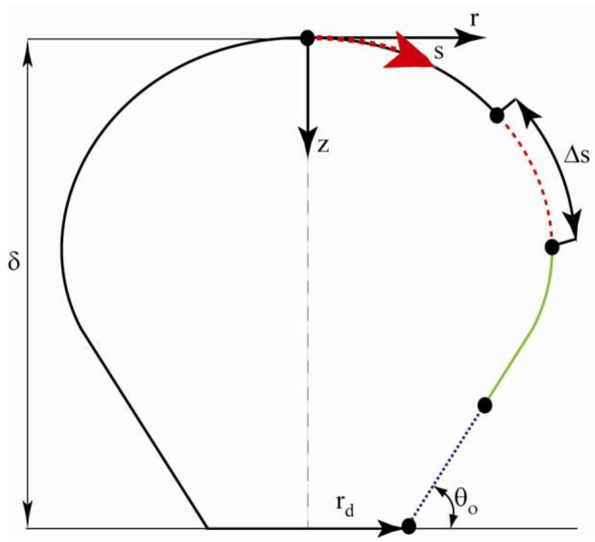

Figure 8. Schematic of the bubble shape, when it is divided into the several parts.

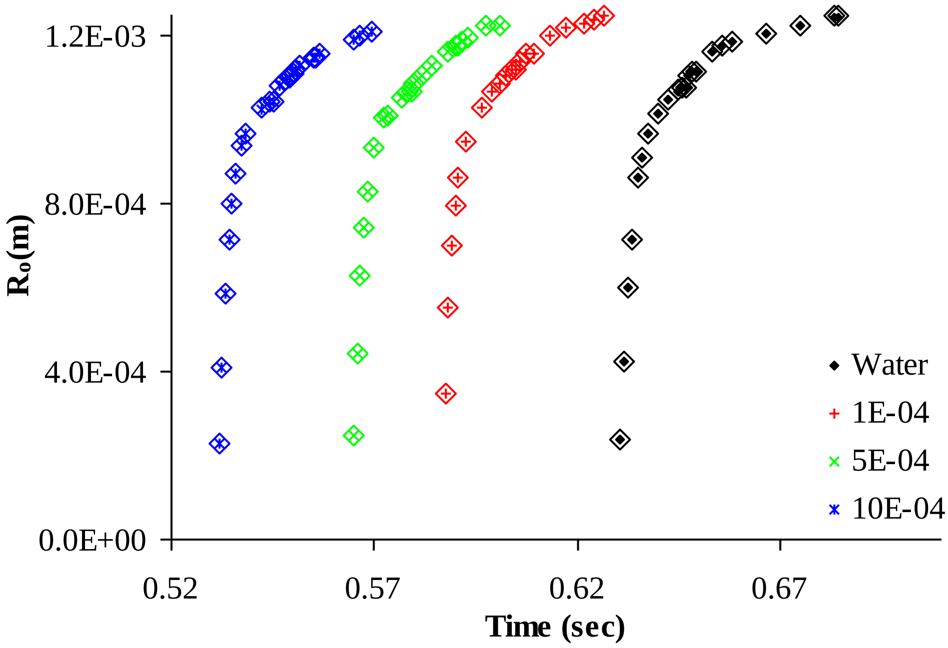

Figure 9. Comparison of radius of curvature at apex predicted by the Young-Laplace equation and analytical expression (19), inside water and gold nanofluid from 0.4 mm stainless steel substrate nozzle, for 0.7 ml/min nominal air flow rate. Three gold nanofluids with concentrations of 1E-4 w, 5E-4 w and 10E-4 w are compared with each other.

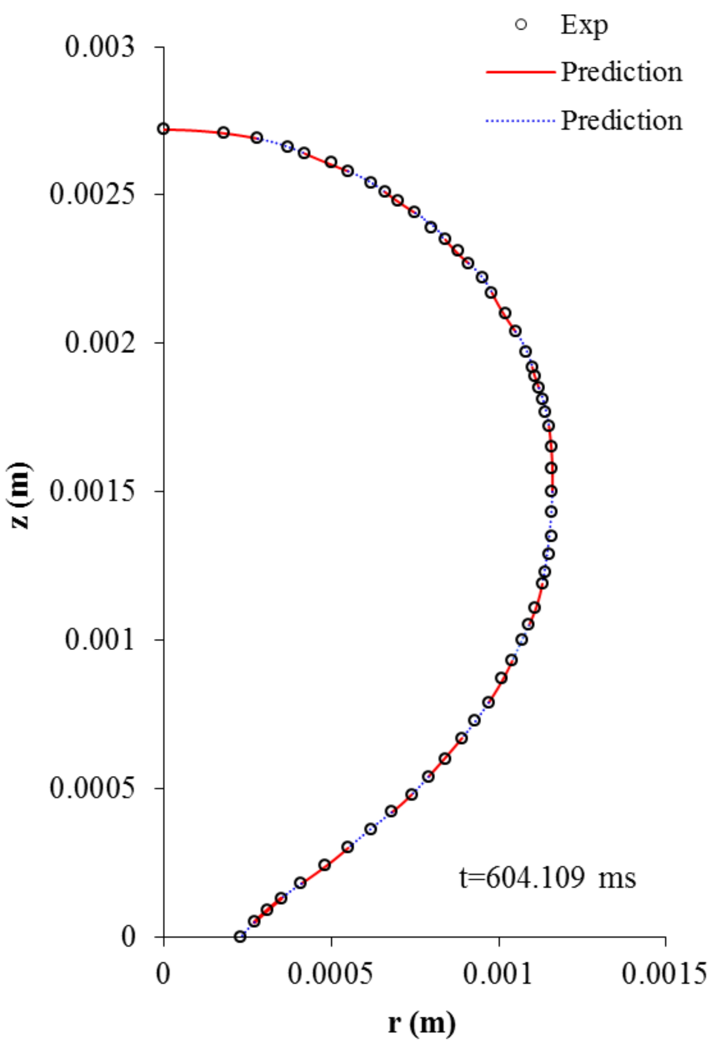

Figure 10. Prediction of bubble shape inside gold nanofluid (1E-4 w) from 0.4 mm stainless steel substrate nozzle for nominal air flow rate of 0.7 ml/min, using system of ordinary differential equations (26, 28-30) along with equation (19) for each individual part.

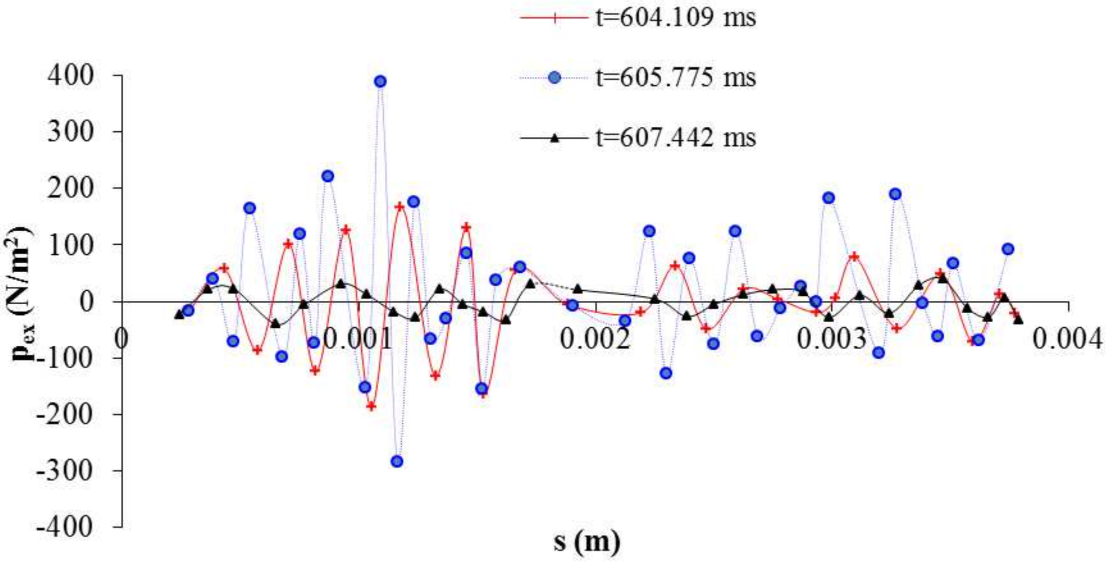

Figure 11. Variation of p_{ex} across the liquid-gas interface, along the bubble perimeter.

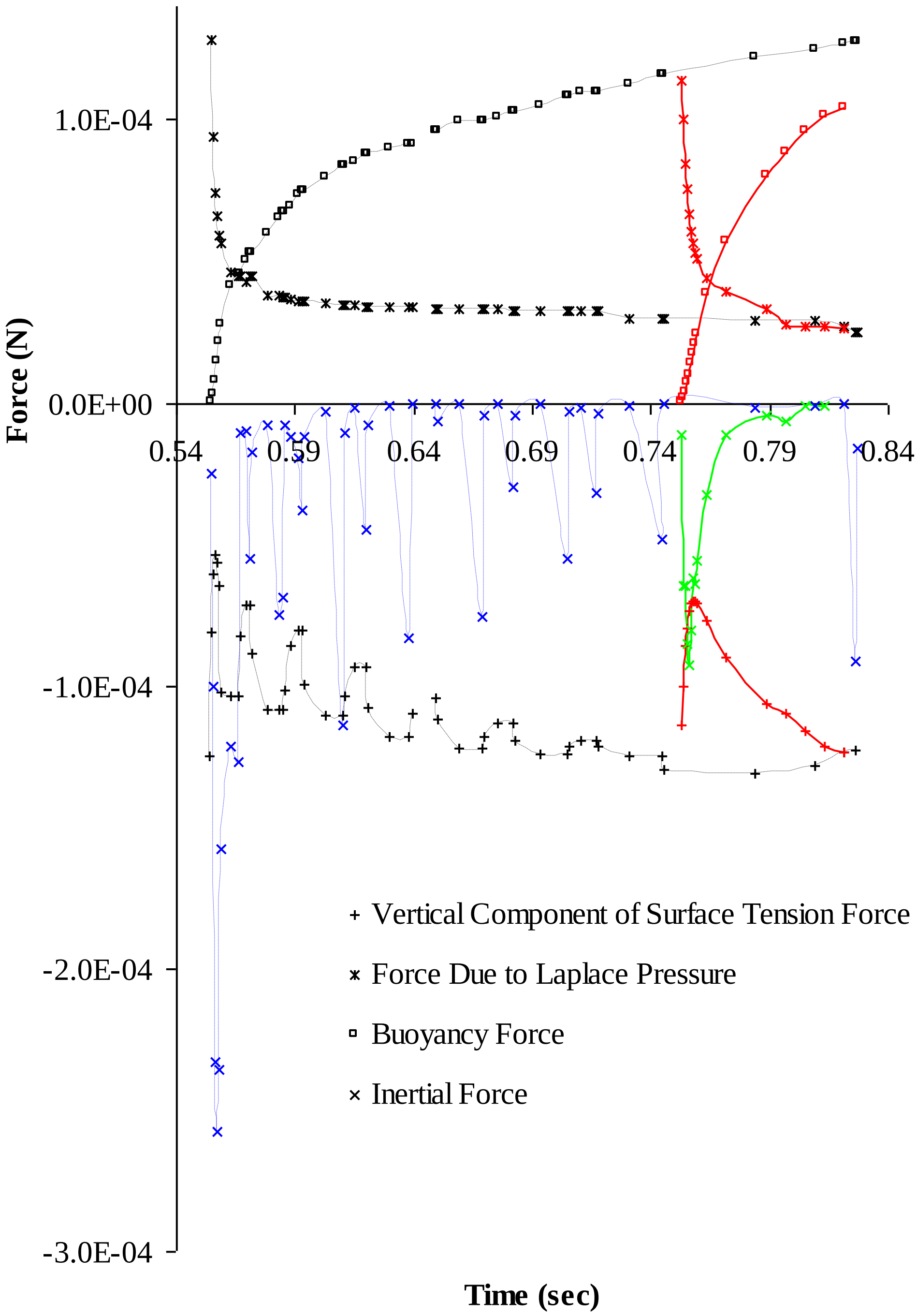

Figure 12. Variation of forces due to Laplace pressure, vertical component of surface tension, buoyancy, and inertial with time inside water from stainless steel needle and substrate nozzles with the same diameter (0.51 mm). The nominal gas flow rate is 0.7 ml/min.

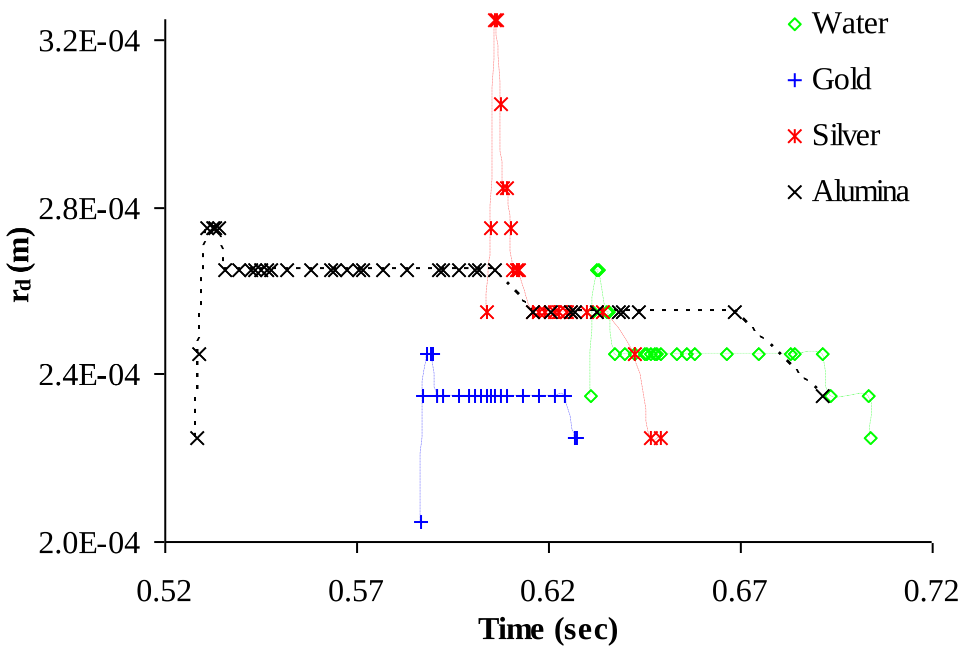

Figure 13. Variation of the radius of triple line with time from the 0.4 mm stainless steel nozzle inside water, gold (1E-4 w), silver (1E-4 w) and alumina (0.37E-4 w) nanofluids for 0.7 ml/min nominal air flow rate [26].

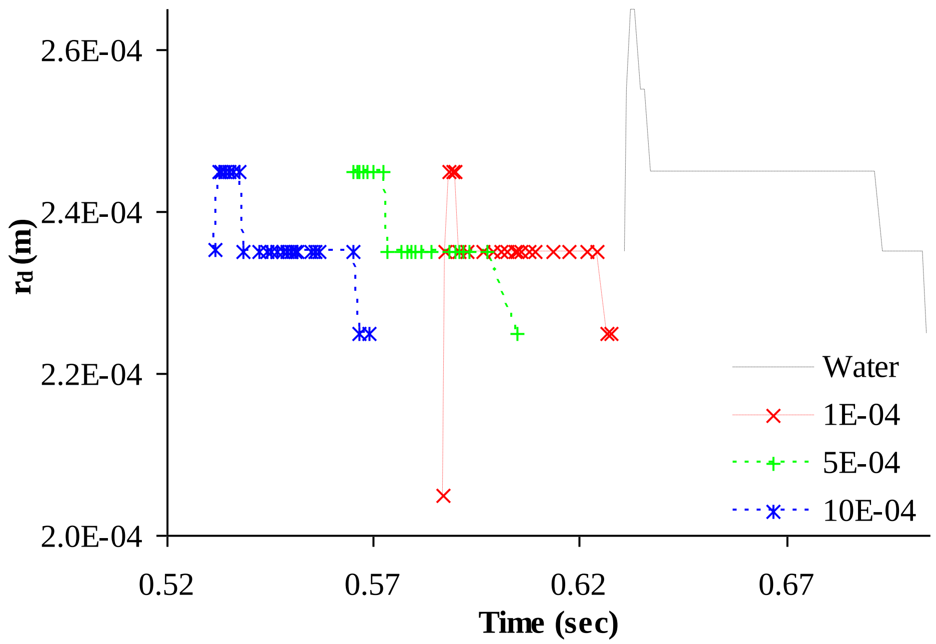

Figure 14. Variation of radius of triple line with time inside water and gold nanofluids from 0.4 mm stainless steel substrate nozzle, for 0.7 ml/min nominal air flow rate. Three gold nanofluids with concentrations of 1E-4 w, 5E-4 w, and 10E-4 w are compared with each other.

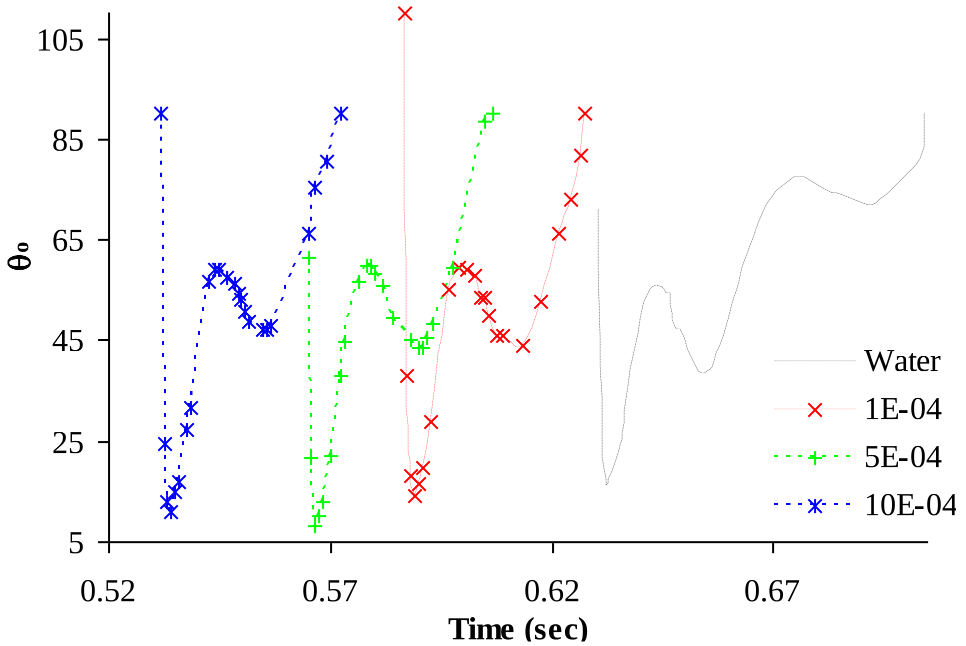

Figure 15. Variation of bubble contact angle with time inside water and gold nanofluids from 0.4 mm stainless steel substrate nozzle, for 0.7 ml/min nominal air flow rate. Three gold nanofluids with concentrations of 1E-4 w, 5E-4 w, and 10E-4 w are compared with each other.